



Heterointegration of Dissimilar Materials

Ravi Droopad
TEXAS STATE UNIVERSITY-SAN MARCOS

07/28/2015
Final Report

DISTRIBUTION A: Distribution approved for public release.

Air Force Research Laboratory
AF Office Of Scientific Research (AFOSR)/ RTD
Arlington, Virginia 22203
Air Force Materiel Command

REPORT DOCUMENTATION PAGE				<i>Form Approved</i> <i>OMB No. 0704-0188</i>	
The public reporting burden for this collection of information is estimated to average 1 hour per response, including the time for reviewing instructions, searching existing data sources, gathering and maintaining the data needed, and completing and reviewing the collection of information. Send comments regarding this burden estimate or any other aspect of this collection of information, including suggestions for reducing this burden, to Department of Defense, Washington Headquarters Services, Directorate for Information Operations and Reports (0704-0188), 1215 Jefferson Davis Highway, Suite 1204, Arlington, VA 22202-4302. Respondents should be aware that notwithstanding any other provision of law, no person shall be subject to any penalty for failing to comply with a collection of information if it does not display a currently valid OMB control number. PLEASE DO NOT RETURN YOUR FORM TO THE ABOVE ADDRESS.					
1. REPORT DATE (DD-MM-YY) 20/07/15		2. REPORT TYPE Final		3. DATES COVERED (From - To) 1 May 2010 – 30 April 2015	
4. TITLE AND SUBTITLE Heterointegration of Dissimilar Materials				5a. CONTRACT NUMBER	
				5b. GRANT NUMBER FA9550-10-1-0133	
				5c. PROGRAM ELEMENT NUMBER	
6. AUTHOR(S) Droopad, Ravi; Lee, Byounggak				5d. PROJECT NUMBER	
				5e. TASK NUMBER	
				5f. WORK UNIT NUMBER	
7. PERFORMING ORGANIZATION NAME(S) AND ADDRESS(ES) Texas State University, 601 University Drive, San Marcos, TX 78666				8. PERFORMING ORGANIZATION REPORT NUMBER	
9. SPONSORING/MONITORING AGENCY NAME(S) AND ADDRESS(ES) Air Force Office of Scientific Research 875 North Randolph Street Suite 325, Rm 3112 Arlington, VA 22203				10. SPONSORING/MONITORING AGENCY ACRONYM(S) AFOSR	
				11. SPONSORING/MONITORING AGENCY REPORT NUMBER(S)	
12. DISTRIBUTION/AVAILABILITY STATEMENT DISTRIBUTION A: Distribution approved for public release					
13. SUPPLEMENTARY NOTES					
14. ABSTRACT The integration scheme for compound semiconductors, functional oxides and silicon has been developed using molecular beam epitaxy with the oxide as a buffer layer on silicon substrates. This scheme will enable multifunctional oxides to be integrated with Si based logic and high speed optoelectronics afforded by III-V compound semiconductors. Various processes were developed whereby functional oxides were epitaxially deposited onto both silicon and compound semiconductor substrates. The oxide/semiconductor interface was studied in an effort to understand the bonding chemistry and the energetics to develop growth processes for 2-dimensional growth of compound semiconductors. Using a combination of high resolution transmission electron microscopy, in-situ XPS and density functional calculation a model of the bonding between the atoms at the SrTiO3/GaAs interface emerge. The relative stability of a number of interfacial structures was compared using the Gibbs free energy and for thin oxide layers, the most energetically stable structure was determined to be As-Sr interface with Sr atoms coming from an oxygen-depleted SrO layer. Using 3 terminations of the oxide surface, compound semiconductor layers were deposited by MBE.					
15. SUBJECT TERMS Heterointegration, epitaxial, functional oxides, compound semiconductors					
16. SECURITY CLASSIFICATION OF:			17. LIMITATION OF ABSTRACT: SAR	18. NUMBER OF PAGES	19a. NAME OF RESPONSIBLE PERSON (Monitor) Kenneth C. Goretta 19b. TELEPHONE NUMBER (Include Area Code) (703) 696-7349
a. REPORT U	b. ABSTRACT U	c. THIS PAGE U			

Standard Form 298 (Rev. 8-98)
Prescribed by ANSI Std. Z39-18

Heterointegration of Dissimilar Materials

Final Report

Ravi Droopad, Byounghak Lee

Summary

Crystalline oxides on semiconductors are becoming increasingly important as more functionality on conventional semiconductor devices is being sought for new applications; integration of Si, functional oxides and compound semiconductors will open the possibility for a compact system-on-a-chip solution for defense and commercial applications. In general, the magnetic and ferroelectric properties of oxides are enhanced with oxide crystallinity. These oxides monolithically integrated onto semiconductors also provide an opportunity for devices development that addresses the CMOS “end of roadmap” concerns. The integration of ferroelectric and ferromagnetic oxides with mature existing semiconductors will enable future generations of logic and memory devices that can be defined and reconfigured using polarization and ferromagnetism.

The objective of this program was to develop a fundamental understanding of the heterointegration of dissimilar materials whereby functional oxides and III-V semiconductors can be monolithically integrated onto silicon substrates. This will enable the fabrication of a system on a chip device incorporating the signal processing capability of Si devices, sensors and/or actuators using functional oxides and the power amplification and transmitting capabilities of III-V semiconductors. While the materials integration was primarily carried out using molecular beam epitaxy we implement various modeling technique to develop an understanding of the interfacial structure that is necessary to develop and modify deposition techniques/processes for high quality heterostructures involving these diverse class of material systems. In particular, we focused on the structural and electronic properties at the oxide/semiconductor interfaces and for the first time deposited epitaxial ferroelectric oxide layers on compound semiconductor that exhibited ferroelectric switching. We have also developed an integration scheme to deposit compound semiconductor and epitaxial oxides on silicon substrates. The following chapters describe the experiments and results obtained during the research phase of this program.

Table of Contents

Summary:	2
Chapter 1: In-situ Photoemission study of the Interfacial Properties of SrTiO ₃ /Si during MBE..	3
Chapter 2: Interface Properties of MBE Grown Epitaxial Oxides on GaAs.....	13
Chapter3: Epitaxial Ferroelectric Oxides on Semiconductors- A route towards negative capacitance devices	23
Chapter 4: Structural Properties of SrTiO ₃ on GaAs(001) Interface.....	31
Chapter 5: Heterointegration of III-V on Silicon using a Crystalline Oxide Buffer Layer.....	41

Chapter 1

In-situ Photoemission study of the Interfacial Properties of SrTiO₃/Si during MBE

ABSTRACT

An in-situ investigation of the interface evolution during MBE deposition of SrTiO₃ on Si has been undertaken using x-ray photoelectron spectroscopy. This study revealed that the critical parameter to control the oxide/semiconductor interface is the incident oxygen during nucleation. Increase in oxygen leads to the formation of interfacial SiO₂ even though the surface as monitored by RHEED remained 2-dimensional; the formation is due to the reaction of Si with oxygen that has diffused through the oxide film. Low oxygen partial pressure leads to unoxidized Ti, a destruction of the interface and the growth of non-crystalline oxide films. The growth of BiFeO₃ on SrTiO₃/Si with excellent crystalline quality was demonstrated which opens the possibility for oxide semiconductor integration leading to new device architectures.

1.1 INTRODUCTION

Semiconductors have been the main driver for the development of the technology responsible for the information age with the proliferation of personal communication devices with increasing computing capabilities. This has been possible due to the aggressive scaling undertaken by the Si industry for complementary metal oxide semiconductor (CMOS) devices. However, it is apparent that Si has reached a point when new materials into the device flow need to be considered. The first was the replacement of the gate dielectric as the thickness of conventional SiO₂ required for the present technology node will result in excessive leakage current due to quantum mechanical tunneling. After years of research and development, Hf-based gate dielectric with metal gates is now being used in CMOS manufacturing. In addition, research are currently being undertaken to replace Si itself as the channel with high mobility compound semiconductors. It is therefore an opportune period, when the addition of more functionality onto semiconductor devices can be given serious considerations to overcome the limitations of Moore's Law with respect to reduced dimensions. Current research in crystalline

oxides has demonstrated that the material properties can be tuned with changes in composition and strain. These properties that include magnetic and ferroelectric ordering, piezoelectricity, pyroelectricity, etc. can be utilized in a variety of new device applications including memory and sensors and as such would be ideal to integrate with semiconductors for new system-on-chip technologies. The properties of the oxides are enhanced with crystallinity and an understanding of the nucleation of various oxides on semiconductors is critical for their integration. Currently, among most studied, and successful, growth of a crystalline oxide on semiconductors has been is the perovskite SrTiO₃ on both Si and GaAs using molecular beam epitaxy [1-4]. This was accomplished by the deposition of a sub-monolayer layer of Sr forming a template [5] that prevents the oxidation of Si when exposed to oxygen during the nucleation of the STO layer. The oxide layer lends itself the growth process that can be accomplished using a layer by layer technique as described by McKee et. al. [1] or co-deposition in which the constituent fluxes of Sr, Ti and O₂ were opened simultaneously [6], the latter used to produce strained STO on Si that exhibit ferroelectricity [7]. While a careful control of the oxygen during nucleation has been demonstrated to produce commensurate growth of SrTiO₃ (STO) on Si, the evolution of the oxide/semiconductor interface including the oxidation states of the various elements in the films are not known. Li et. al. [6] and more recently Niu et. al. [8] have demonstrated the need for a low nucleation temperature under moderately low oxygen pressure in order to obtain a sharp oxide/semiconductor interface. In this study the use of *in-situ* photoemission spectroscopy to investigate of the SrTiO₃/Si interface is undertaken to determine the formation of interfacial SiO₂ and the oxidation states of the various cations including Ti at various oxygen partial pressures during the initial stages of growth and correlate the results with RHEED observations. In addition SrTiO₃ on Si can be used as virtual substrates for the growth of other functional oxides. However, in most cases these oxides require the use of high oxygen pressures and/or atomic species to completely oxidize the cations and mitigate oxygen vacancies. The results of the growth of BiFeO₃, a multiferroic materials exhibiting both ferroelectric and antiferromagnetic ordering, on SrTiO₃ will be described with the effects of such high oxygen pressures on to the oxide/semiconductor interface.

1.2 EXPERIMENTAL

The deposition of SrTiO₃ on Si was carried out in a DCA M600 MBE chamber which is part of a multi-chamber system that also consists of an X-ray photoemission spectroscopy (XPS) analysis chamber, in addition to III-V and II-VI MBE chambers. All chambers are interconnected through an ultra high vacuum buffer chamber allowing for the analysis of the growth process at any stage in the deposition process, even layer-by-layer on samples by transferring to the analysis chamber without exposure to atmosphere. The base pressure in the growth chamber was maintained at $< 5 \times 10^{-10}$ torr. Elemental Sr (low temperature) and Ti (high temperature) in effusion cells were used as sources along with ultra high purity oxygen introduced through a RF plasma source and controlled with a leak valve. During the SrTiO₃ growth the plasma source is switched off to allow us to use molecular oxygen species. The MBE chamber is also equipped with reflection high energy electron diffraction (RHEED) to monitor the surface quality, oxide surface stoichiometry and growth rates, and a crystal monitor to measure fluxes. Temperatures were determined using an optical pyrometer. The XPS analysis chamber consists of a 200 mm hemispherical analyzer (Scienta SES 2002) and a dual anode X-ray source. In order to enhance the surface sensitivity, the electrons projected by the Mg K_α source are collected at an angle of 54° with respect to the surface normal. The electron energy analyzer is operated at high resolution mode (20 eV pass energy) in order to resolve small chemical shifts and other closely spaced spectroscopic features.

The samples used in this study were deposited on (001) oriented 3 inch silicon wafers loaded onto In-free moly holders. The substrates were first subjected to an ultraviolet (UV) ozone treatment prior to being loaded into a load lock where they were outgassed at 150 °C before moving into the growth chamber; the advantage of treating the wafers with ozone is the complete removal of carbon contamination during oxide removal as evidence by the absence of SiC RHEED features after oxide removal. In addition, XPS analysis of the Si substrate after oxide removal detected no C species. The sticking coefficients of both Sr and Ti on Si are unity at the SrTiO₃ growth temperature, so it is imperative the fluxes of each element be calibrated carefully to ensure stoichiometric SrTiO₃ films. The procedure to calibrate the fluxes involved monitoring the RHEED reconstruction during the homoepitaxial growth of SrTiO₃. Sr- or Ti-rich growth is indicated by a 2-fold reconstruction along the SrTiO₃ [110] and the [210] azimuth respectively. The cell temperatures were adjusted so that growth proceeds with a (1x1) surface

reconstruction. Once stoichiometric SrTiO₃ was achieved, periodicity of RHEED oscillations was measured to obtain the oxide growth rate. The growth rate used for the oxide in this study was 1ML or $\sim 3.9 \text{ \AA}/\text{min}$.

The native SiO₂ was removed using a low temperature process involving the deposition of Sr metal on the SiO₂/Si surface and heating to around 750 °C as described in ref [4]. In this study, the initial nucleation of SrTiO₃ was started after the substrate was reduced to about 200 °C. The surface was then exposed to molecular oxygen at various pressures ranging from 1×10^{-8} torr to 1×10^{-6} torr as measured by the chamber pressure (even though the actual incident oxygen flux could be much larger). Immediately after exposure to oxygen of the required pressure, oxide growth was initiated by simultaneously opening both Sr and Ti shutters. After the growth of 3 unit cells or $\sim 12 \text{ \AA}$ of SrTiO₃ the samples were transferred into the analysis chamber for XPS measurements. Once the analysis was done some of the samples were transferred back to the chamber to continue growth of SrTiO₃. *Ex-situ* characterization such as high resolution transmission electron microscopy (TEM), x-ray diffraction (XRD) and atomic force microscopy (AFM) were carried out to analyze the surface and structural quality of the sample.

The growth of BiFeO₃ (BFO) on the SrTiO₃ surface was carried out using Fe and Bi from effusion cells together with atomic oxygen. After the growth of the 200 Å STO layer at 550 °C, the oxygen plasma was switched on with an oxygen partial pressure of 5×10^{-6} torr. The growth was controlled by the arrival rate of the Fe atoms with the Bi flux is supplied in overpressure. The growth rate was determined to be approximately 5Å/min. The BiFeO₃/SrTiO₃/Si was also characterized using x-ray diffraction.

1.3. RESULTS AND DISCUSSIONS

After the clean Si, displaying a (2x1) surface reconstruction at 800 °C, was cooled to 450 °C the RHEED pattern displayed a mixture of 2x and 3x reconstruction representing a 2 –domain (3x2) surface structure shown in figure 1(a). Additional Sr was then deposited until a well ordered clean (2x1) RHEED pattern re-emerged, representing a surface coverage of $\frac{1}{2}$ ML, figure 1(b) [9]; this surface reconstruction served as a template for the growth of SrTiO₃. After the template formation the substrate temperature was reduced to initiate growth. This template layer protects the Si from oxidizing during the introduction of molecular oxygen and has a surface energy that

is thermodynamically favorable for the growth of 2D STO [6] resulting in the nucleation of the

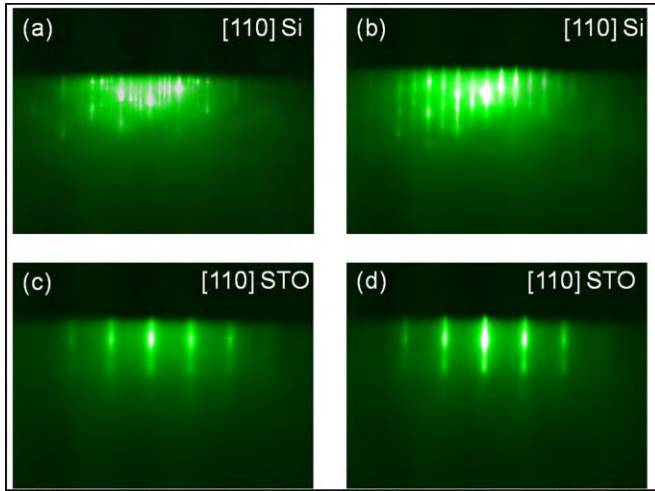


Figure 1: RHEED pattern recorded sequentially during SrTiO₃ growth on Si (a) Si surface after cleaning (b) Si surface after ½ ML of Sr template (c) 3 ML of SrTiO₃ grown at optimal conditions (d) 3 ML of SrTiO₃ grown at optimal conditions on Si after anneal.

crystalline SrTiO₃ layer on Si. There are three main parameters which contribute to or control the two dimensional nucleation of SrTiO₃ on silicon: (i) Sr and Ti fluxes, (ii) the growth temperature, and (iii) the oxygen pressure. The fluxes were calibrated prior to growth as discussed before. The optimal growth temperatures have been shown to be in the range from 200-550 °C. Although high temperatures in the range of 500 °C leads to better crystallization of SrTiO₃, it also leads to

oxidation of the underlying Si forming SiO₂ or other forms of silicates due to the higher reactivity of oxygen with Si. At low temperatures, with the presence of the Sr template and at the optimum oxygen pressure it is possible to form abrupt crystalline interfaces.

After the growth of the first 3 ML all samples were annealed at about 550 °C with the oxygen turned off and the chamber pressure was $< 5 \times 10^{-9}$ torr. Although *ex-situ* analysis of fully grown heterostructures has been carried out before [10-11], here the focus was mainly on the conditions that affect the formation of SiO₂ at the STO/Si interface. Comparisons were made on the detailed analysis of the evolution of the RHEED patterns and XPS data, with respect to the oxygen pressure used during each sample run.

A comparison of four samples (i), (ii), (iii) and (iv) in which oxygen pressures used during nucleation of SrTiO₃ were of 2×10^{-8} , 5×10^{-8} , 1×10^{-7} and 6×10^{-7} torr respectively. Figure 1(c) and 1(d) shows a typical RHEED surface reconstruction, taken along the SrTiO₃ [110] azimuth, after growth and anneal respectively, of sample (i) i.e. 3 unit cell SrTiO₃ film on Si (100) under optimized oxygen pressure of around 2×10^{-8} torr. In case of Sample (ii) where the oxygen pressure was increased only slightly, the RHEED patterns showed no significant changes. However, when the oxygen pressure was changed to $\sim 1 \times 10^{-7}$ torr (Sample (iii)) during the start of oxide deposition, the RHEED streaks started to get more and more diffused and one

point disappeared during growth but recovered and re-appeared during annealing at 550 °C for 15 minutes. Finally for sample (iv) with the increased oxygen level of $\sim 6 \times 10^{-7}$ torr the RHEED streaks started to get diffused rapidly and eventually disappeared. For this sample, the RHEED features only partially recovered after anneal yielding poor quality SrTiO₃ layer.

Figure 2 shows XPS spectra of Si 2*p* taken on the four samples (i-iv) used in this study. The data clearly shows the effects of initial oxygen pressure on the formation of SiO₂ during growth of SrTiO₃ on Si. Even though RHEED features showed no apparent differences when comparing (i) and (ii), there is evidence of a very thin layer of SiO₂ in case of sample (ii). Even though the RHEED streaks fully recover in case of Sample (iii), there is strong SiO₂ peak and such growth conditions have been shown to yield a thin amorphous layer between the crystalline SrTiO₃ and the Si substrate. Figure 3 shows a TEM micrograph of the interface for sample (i) which shows a crystalline transition between the Si substrate and the SrTiO₃ film. Based on the XPS measurements the bonding arrangement the oxide/semiconductor interface comprise of Si-Sr-O bonds with no direct Si-O bonds.

While it is possible to nucleate single crystal SrTiO₃ directly on a Si substrate provided the ½ ML Sr template is present, the growth of thick SrTiO₃ films invariably results in a layer of SiO₂ formation at the interface due to the reaction of interfacial silicon with oxygen that has diffused during growth. The thickness of the interface layer increases with growth temperature and oxygen partial pressure; with a faster increase when a more reactive atomic oxygen or ozone is used. Figure 3 shows a TEM image of SrTiO₃ layer grown at 550 °C with an oxygen pressure of 1×10^{-6} mbar. With careful control however, SrTiO₃ layers as thick as 40 Å have been

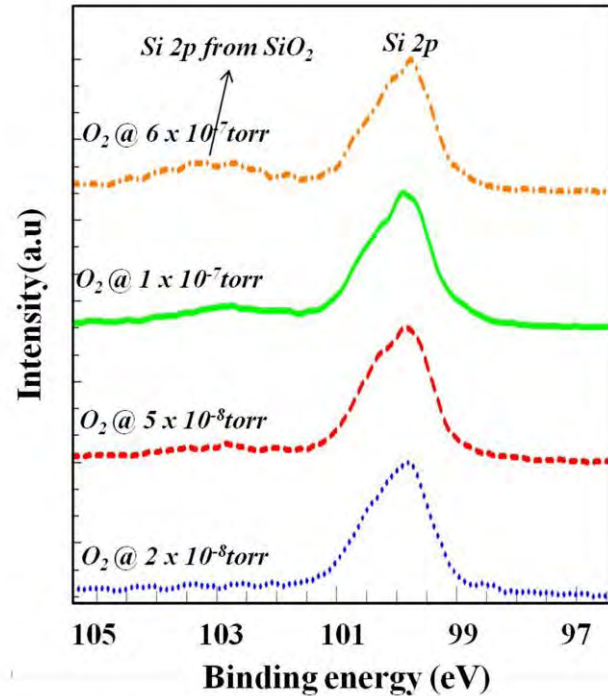


Figure 2: : Si 2*p* XPS spectra showing the effects of initial oxygen on the formation of SiO₂ during SrTiO₃ growth on Si.

deposited with a sharp interfacial transition between Si and the oxide layer. The formation of the amorphous SiO₂ occurs after and during the growth of crystalline SrTiO₃ not evident using by RHEED observations which is sensitive only to the topmost 1 or 2 monolayers. The reaction of

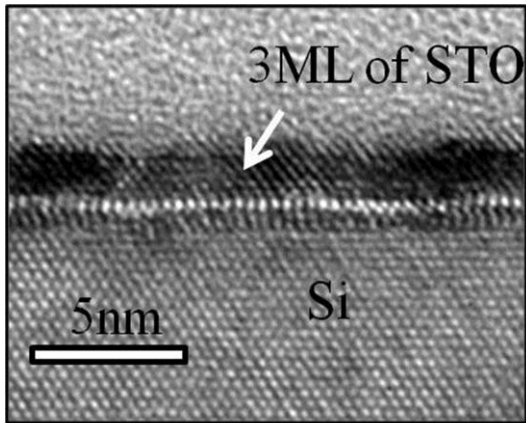


Figure 3: High resolution TEM micrograph of 3 ML SrTiO₃ on Si grown under optimized conditions

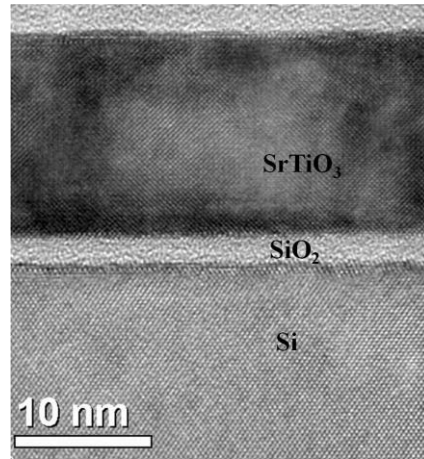


Figure 4: High resolution TEM micrograph showing the SiO₂ interface of a relatively thick single crystal SrTiO₃ film grown on Si

interfacial Si with oxygen that diffuses through the SrTiO₃ films during growth or post growth anneal is responsible for the SiO₂ layer, the thickness of which depends on the deposition temperature, the oxygen partial pressure and the oxygen species used (molecular, atomic). The TEM micrograph of figure 4 shows the SiO₂ interface of a relatively thick single crystal STO film grown on Si that nucleated using the process described in this paper but with an increased temperature and incident oxygen for the bulk of the film.

Along with the criteria of preventing Si oxidation, it is also important to ensure that the initial SrTiO₃ layers that are formed is stable and has the right compositional ratio between SrO and TiO₂. Figure 5 shows XPS spectra of Ti-2p core level of samples grown at different growth conditions. Figure 5(a) is a Ti 2p XPS spectra of SrTiO₃ grown by co-

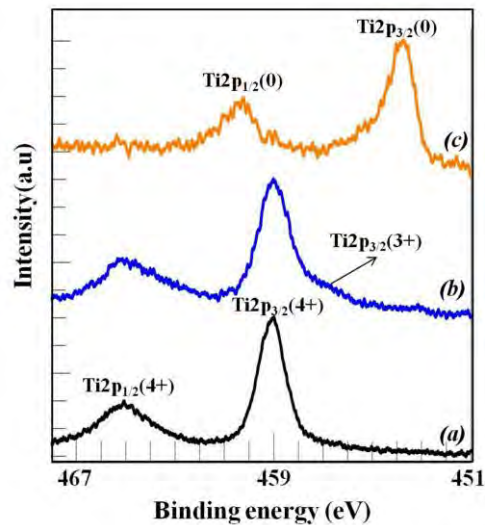


Figure 3: XPS spectra of Ti 2p core level from SrTiO₃ grown under (a) optimized growth condition, (b) Low oxygen pressure (< 2x10⁻⁸ torr) and (c) Non-optimized growth condition

deposition of Sr and Ti at optimized growth conditions, i.e. O_2 pressure was at 2×10^{-8} torr and Sr and Ti were calibrated to produce stoichiometric $SrTiO_3$ as confirmed by RHEED. The single peak position is indicative of fully oxidized Ti metal. However, if the oxygen pressure is reduced lower than the required pressure ($< 1 \times 10^{-8}$ torr), the result is a partial oxidation of Ti giving rise to a shoulder at lower binding side of the Ti $2p_{3/2}$ peak indicative of some amount Ti^{3+} oxidation states as shown in figure 5(b). In addition, when the growth is carried out under non-optimized conditions, where in both the oxygen partial pressure and the ratio of Ti and Sr are far from ideal there is evidence of metallic Ti ($Ti\ 2p_{3/2}(0)$) as shown in figure 5(c). In this case there is also evidence of SiO_2 formation at the oxide/Si interface as a result of non 2-dimensional deposition. The RHEED features became spotty and completely disappeared and did not recovered upon annealing.

$BiFeO_3$ growth has been accomplished on the $SrTiO_3/Si$ with excellent crystallinity and stoichiometry. The crystallinity of the $BiFeO_3$ films were confirmed by x-ray diffraction and shown in the theta-2theta scan in figure 6 which suggests a (100) oriented $BiFeO_3$ films. The full width at half maximum of the $BiFeO_3$ (002) peak is 595 arcsec. The inset of figure 6 shows the RHEED pattern after the growth of 300 Å $BiFeO_3$ on a 200 Å $SrTiO_3$ layer that has been deposited on Si displaying a strong 6x reconstruction along the [110] direction. The starting RHEED pattern for the $SrTiO_3$ surface displayed a (1x1) reconstruction which evolved into a 3 fold and finally to a 6x reconstruction along the [110] azimuth.

1.4. CONCLUSIONS

The interfacial properties between $SrTiO_3$ and Si were determined *in-situ* by x-ray photoemission spectroscopy by investigating the formation of SiO_2 and the oxidation states of the cations during MBE deposition. The parameters affecting the

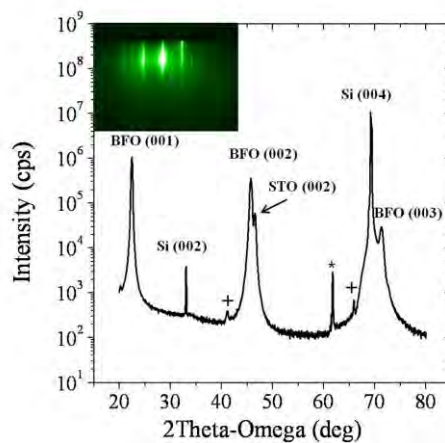


Figure 4: Theta-2theta x-ray diffraction scan of a 300 Å $BiFeO_3$ film grown epitaxially on a $SrTiO_3/Si$ substrate by MBE. The peak labeled with a * is the $Si(004)$ contribution from the $Cu\ K_{\beta}$ line, while those labeled with a + are the K_{β} contribution from the $SrTiO_3$ layer. The inset shows the RHEED pattern after the growth of the $BiFeO_3$ layer.

interface during the initial nucleation of the oxide layer were determined and the oxygen partial pressure was found to be critical parameter in controlling the crystallinity of the interface. While parameters have been identified to control the interface during nucleation, the growth of thick oxide films invariably results in the formation of an interfacial SiO₂ layer due to the diffusion of oxygen during growth at the conditions required for improved crystal quality and reduced oxygen vacancies. This is also the case when other functional oxides are grown on Si using SrTiO₃ as the enabling buffer layer, since for some oxides the use of activated oxygen available from a plasma source or ozone is required for the complete oxidation of the elements and reduction of oxygen vacancies. The SrTiO₃/Si has been used as a virtual substrate to deposit BiFeO₃, a functional multiferroic oxide layer creating a pathway for integration of these oxides with Si substrates.

REFERENCES

- [1] R. McKee, F. Walker and M. Chisholm, *Phys. Rev. Lett.* **81**, 3014 (1998).
- [2] R. Droopad, Z. Yu, H. Li, Y. Liang, C. Overgaard, A. Demkov, X. Zhang, K. Moore, K. Eisenbeiser, M. Hu, J. Curless and J. Funder, *J. Cryst. Growth.* **251**, 638 (2003).
- [3] J. H. Haeni, C. D. Theisd and D. G. Schlom, *J. Electroceramics.* **4:2/3**, 385 (2000).
- [4] Y. Wei, X. Hu, Y. Liang, D. C. Jordan, B. Craigo, R. Droopad, Z. Yu, A. Demkov, J. L. Edwards, Jr., and W. J. Ooms, *J. Vac. Sci. Technol. B* **20**, 1402 (2002).
- [5] R. A. McKee, F. J. Walker, and M. F. Chisholm, *Science.* **293**, 468 (2001)
- [6] H. Li, X. Hu, Y. Wei, Z. Yu, X. Zhang, R. Droopad, A. A. Demkov, J. Edwards, K. Moore, W. Ooms, J. Kulik, and P. Fejes, *J. Appl. Phys.* **93**, 4521 (2003).
- [7] M. P. Warusawithana, C. Cen, C. R. Slesman, J. C. Woicik, Y. L. Li, L. F. Kourkoutis, J. A. Klug, H. Li, P. Ryan, L. P. Wang, M. Bedzyk, D. A. Muller, L. Q. Chen, J. Levy, and D. G. Schlom, *Science.* **324**, 367 (2009).
- [8] G. Nui, W. W. Peng, G. Saint-Girons, J. Penuelas, P. Roy, J. B. Brubach, J-L. Maurice, G, Hollinger, B. Vilquin, *Thin Solid Films.* **519**, 5722 (2011)
- [9] X. Hu, Z. Yu, J. Curless, R. Droopad, K. Eisenbeiser, J. Edwards, W. Ooms, D. Sarid, *Appl. Surf. Sci.* **181**, 103 (2001).
- [10] G. Niu, B. Vilquin, J. Penuelas, C. Botella, G. Hollinger, and G. Saint-Girons, *J. Vac. Sci. Technol. B* **29**, 041207 (2011).
- [11] G. Niu, J. Penuelas, L. Largeau, B. Vilquin, J. L. Maurice, C. Botella, G. Hollinger, and G. Saint-Girons, *Phys. Rev. B* **83**, 054105 (2011).

Chapter 2

Interface Properties of MBE Grown Epitaxial Oxides on GaAs

ABSTRACT

Single crystal SrTiO₃ layers were grown on GaAs using both molecular and atomic oxygen and the interfaces were probed using room temperature photoluminescence and *in-situ* x-ray photoemission spectroscopy. The increase in PL intensity for the oxide/GaAs structure in which molecular oxygen was used suggest a decrease in the density of interfacial defects resulting in some level of Fermi level unpinning. When atomic oxygen was used during growth the interface appears to have an increase in the density of defects and a pinned Fermi level similar to that for a GaAs layer with a native oxide. X-ray photoemission measurements indicate an increase in the Ga-O bonding at the interface when the plasma source was used with an addition of As-As bonding not present in the sample grown using molecular oxygen. These results suggest the possibility of using a crystalline oxide as a gate dielectric in III-V MOSFET devices.

2.1 INTRODUCTION

Heteroepitaxy of oxides on semiconductors offer the potential for a controlled interface with low defects and as an enabler for the integration of oxide-based functionality on both silicon and III-V devices. Control at a high-k dielectric/compound semiconductor interface to mitigate Fermi level pinning is becoming critical as high mobility materials are currently being considered for the channel in future generations of Si complementary metal oxide semiconductor (CMOS) devices. In addition to being used as potential gate dielectrics, epitaxial oxides also serve as pathways for the integration of novel functional devices incorporating other oxides with multiferroic properties, i.e. oxide exhibiting both ferromagnetic and ferroelectric properties with high speed optoelectronics afforded by compound semiconductors. Molecular beam epitaxy (MBE) has proven to be a versatile growth process for the deposition of high quality epitaxial oxides on silicon, viz. SrTiO₃ (STO) with controlled semiconductor/oxide interface. The deposition parameters can be controlled to tailor the interfacial layer allowing for commensurate

growth when grown on Si [1-3]. Depending on the growth conditions, a SiO₂ layer can also be formed at the interface between the oxide and Si. The successful deposition of an epitaxial oxide on compound semiconductors with a crystalline transition across the interface can potentially be used as gate dielectrics in metal oxide semiconductor field effect (MOSFET) devices. However crystalline perfection of the interface is not the only requirement; the interface state densities need to be low enough to unpin the Fermi level allowing for unrestricted modulation of the Fermi level with gate voltage.

Epitaxial growth of oxides on GaAs has been the subject of research for over 2 decades. Among the first reported oxide growth on GaAs was carried out by laser MBE and involved the growth of MgO on different terminated GaAs surfaces [4, 5]. The resultant films consisted of textures and columnar grains. Hong and co-workers [6] used electron beam evaporation to deposit cubic gadolinium oxide on GaAs for application as a gate dielectric in which capacitance-voltage measurements was used to demonstrate both inversion and accumulation in diode structures. More recently, atomic layer deposition was used to deposit crystalline BeO thin films on both Si and GaAs [7] also for high-k dielectric applications with x-ray diffraction (XRD) showing that different crystal structures of BeO exist in the film. MBE was also used to successfully deposit STO on GaAs and structural characterization determined that the interface was void of any amorphous interfacial layer [8]. By analyzing the STO/GaAs interface by x-ray photoelectron spectroscopy (XPS) and transmission electron microscopy (TEM), Klie et. al. concluded that when STO is grown directly on GaAs, the result is a pinned Fermi level [9]. However, the use of a ½ monolayer Ti pre-layer prior to the deposition of the STO layer results in a Fermi level that is unpinned. In this study, we will investigate the interfacial properties of single crystal STO on GaAs as a function of oxygen species during the bulk of the STO growth with the goal of determining the quality of the interface with respect to Fermi level pinning. The initial nucleation of the oxide film, in all cases will be carried out using molecular oxygen and the atomic oxygen used only after the 2nm of STO has been grown. It has been shown that using high oxygen fluxes or atomic oxygen during the MBE growth of STO on Si that a layer of SiO₂ is formed at the interface due to oxygen diffusion through the oxide film reacting with interfacial Si. It is not clear what the effect of using atomic oxygen during STO growth on GaAs will have on the oxide/semiconductor interface. The defect density at the oxide/GaAs interfaces using both molecular and atomic oxygen, generated from a plasma source, will be explored qualitatively

using room temperature photoluminescence measurements. These results will be correlated with *in-situ* XPS measurements.

2.2. EXPERIMENT

All layer growths are carried out in a multichamber UHV system incorporating MBE chambers for compound semiconductors and oxides in addition to a photoemission spectroscopy chamber that is used for probing the surfaces and interfaces. This configuration allows for the wafers to be transferred into the various chambers without exposure to atmosphere. This is important as it ensures that the surface remained clean and well ordered for subsequent deposition and eliminates artifacts during spectroscopic analysis. The solid source III-V chamber has a base pressure of $<5 \times 10^{-10}$ mbar pumped using a combination of ion and cryogenic pumping. Growth rates are determined using the typical reflection high energy electron diffraction (RHEED) oscillation technique and the substrate temperature is measured using an optical pyrometer that was cross referenced using a KSA bandit system. The oxide chamber is configured with 2 electron beam evaporators, 7 effusion cells, an oxygen plasma source and pumped using a combination of a 1000 l/s turbo pump and a cryo pump achieving a base pressure of $<5 \times 10^{-10}$ mbar. Sr and Ti metals from effusion cells and high purity oxygen were used as deposition sources. During growth using molecular oxygen, the plasma source is switched off. For the samples grown using oxygen plasma, a power of 300W was used. The oxygen flux was measured using the chamber ion gauge which was independently determined to be the pressure of the incident oxygen flux onto the substrate using a beam flux monitor. A quartz crystal monitor was used for flux determination but oxide stoichiometry and growth rates were determined using RHEED during growth on an STO substrate.

GaAs layer was grown at a substrate temperature of 580°C and a growth rate of 0.8 MLs/sec. To facilitate optical measurements the GaAs structures included a 1.5 μm n-GaAs layer doped at a level of $2 \times 10^{16} \text{ cm}^{-3}$ grown on an n+ substrate. The wafers were then cooled under an As flux until the temperature is $<300^\circ\text{C}$ after which the As cracker valve was closed. After the growth of the III-V layer, the wafers were transferred into the oxide chamber for heteroepitaxy. Once in the oxide chamber, a ½ ML Ti was deposited onto the c(4x4) As stabilized GaAs surface at 300°C. The nucleation of the oxide layer was always carried out using a low flux of molecular oxygen to prevent the oxidation and the disruption of the Ti-templated GaAs surface. The use of

a plasma source during nucleation is detrimental to the nucleation of a crystalline layer as such active oxygen species will have a tendency to oxidize the GaAs surface creating amorphous Ga and As oxides. These amorphous Ga and As-oxides prevent the nucleation of crystalline oxide films. For the investigation of the growth using oxygen plasma, the first 2 nm of STO is grown using molecular oxygen while the subsequent 8 nm was deposited using atomic oxygen generated by switching on the plasma source. The aim was to provide similar nucleation of the oxide layers for both types of samples and only change the oxygen species during the bulk of the STO growth. This would allow us to study the effect of the diffusion of the highly reactive oxygen species on the interfacial properties. The oxide nucleation comprised of co-deposition of Sr, Ti and oxygen at a level of $1-3 \times 10^{-8}$ mbar and a substrate temperature of 300°C for a total thickness of 1 unit cell or $\sim 4\text{\AA}$. This was followed by an annealing at 500°C for 3 minutes after which co-deposition of STO was continued at 500°C until the desired thickness was achieved. RHEED is used throughout the growth to ensure stoichiometric oxide growth.

The oxidation states and chemical bonding at the interface were probed using in-situ x-ray photoemission spectroscopy using a Scienta SES 2002 hemispherical analyzer and a dual anode x-ray source. The structural properties of the films were characterized using *in-situ* RHEED and *ex-situ* x-ray diffraction. The surface morphology was mapped using AFM with a Si probe tip and the optical properties of the interface was investigated using room temperature photoluminescence with an argon ion laser as the excitation source. The incident laser power was 200mW and the PL signal was collected and passed through a 0.85m double pass monochromator with a slit width of 400 μm and collected using a photomultiplier tube.

2.3 RESULTS AND DISCUSSIONS

The nucleation of oxide on GaAs needs to be kinetically favorable to prevent the excessive oxidation of the GaAs sub-surface layer which is a necessary condition for creating an interface with low defects. In this study, the $\frac{1}{2}$ ML of Ti deposited at 300°C was used as the template for the STO nucleation. During the Ti deposition the surface reconstruction changed from a $c(4 \times 4)$ to a (2×1) . Figure 7(a) and (b) shows the RHEED patterns along the GaAs $[\bar{1}10]$ and $[010]$ azimuth respectively of the $c(4 \times 4)$ As stabilized surface at 300°C. After the deposition

of the Ti prelayer the surface reconstruction changed to a (2x1) structure with the RHEED pattern shown in figure 7(c) and (d) along the $[\bar{1}10]$ and $[010]$ showing that the surface remained well ordered even though there was a slight increase in the background intensity. At this stage the oxygen was introduced into the chamber to a level of $1-3 \times 10^{-8}$ mbar after which the Sr and Ti shutters were opened. After the deposition of 1 unit cell of STO, the oxygen was closed and the substrate was heated to 500°C and annealed for 3 mins. The growth of the STO layer was then continued using co-deposition but with a higher molecular oxygen level of 1×10^{-7} mbar. Figures 7(e) and (f) show the RHEED

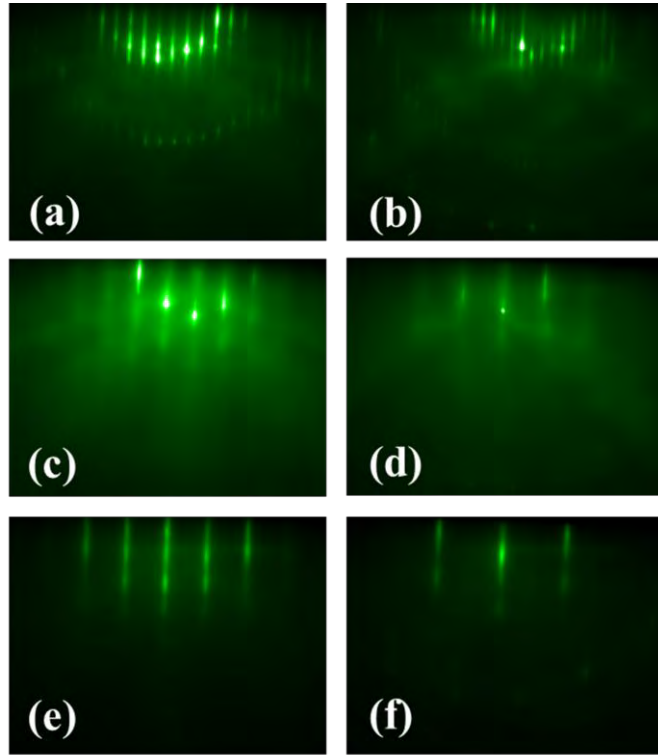


Figure 5: RHEED patterns observed during the growth of STO on GaAs showing the As-stabilised $c(4 \times 4)$ surface along (a) the $[\bar{1}10]$ and (b) the $[010]$ azimuths. After the Ti prelayer is deposited the RHEED patterns (c) along the $[\bar{1}10]$ and (d) the $[010]$ are observed. (e) and (f) shows the RHEED patterns along the $[110]$ and the $[210]$ respectively after the deposition of 100 \AA STO.

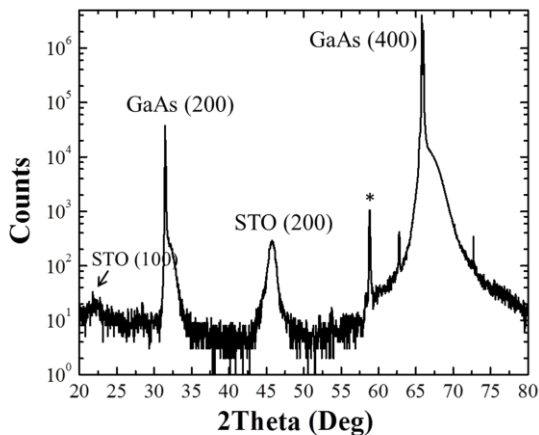


Figure 6: XRD theta-2theta scan of the STO on GaAs showing (100) oriented oxide film. The * represent a peak from the x-ray k_β emission.

pattern along the STO $[110]$ and $[210]$ azimuths respectively after the deposition 100 \AA STO layer on GaAs displaying characteristics of a well ordered and smooth surface. For the growth of the STO layer using atomic oxygen, the plasma source was switched on after the growth of 2 nm oxide with molecular oxygen using a power of 300W. There was no difference in the RHEED patterns during growth using the two oxygen

species. Atomic force measurements show that the STO surface grown using molecular oxygen was 0.51nm with a slightly higher value of 0.68 nm when oxygen plasma was used during growth. The crystal properties of the STO/GaAs were determined by XRD. Figure 8 shows the theta-2theta scan for the film grown using oxygen plasma, indicating (100) oriented STO films. Pole figure measurements confirmed that the STO crystal is rotated 45% in plane to create a 2.3% lattice mismatch with GaAs. The peak positions for the samples grown using molecular oxygen were identical. The difference between the oxide layers manifested itself in the rocking curve of the STO (002) peak which was slightly smaller for that grown using the oxygen plasma source. A value of 0.4° for FWHM is indicative of a high crystalline quality for a 100Å thick STO layer.

Room temperature photoluminescence (PL) measurements can be used to determine the relative properties of the oxide/GaAs interface. This is especially useful for oxides that have small conduction band offsets with the semiconductors which would result in large leakage current when the standard capacitance-voltage measurements are used. Interface traps acts as non-radiative recombination centers and the area under the PL spectrum can, to first order give an indication of the oxide/GaAs interface quality [10]. While PL measurements alone do not indicate the level of interfacial defects, it can be used to provide qualitative information of

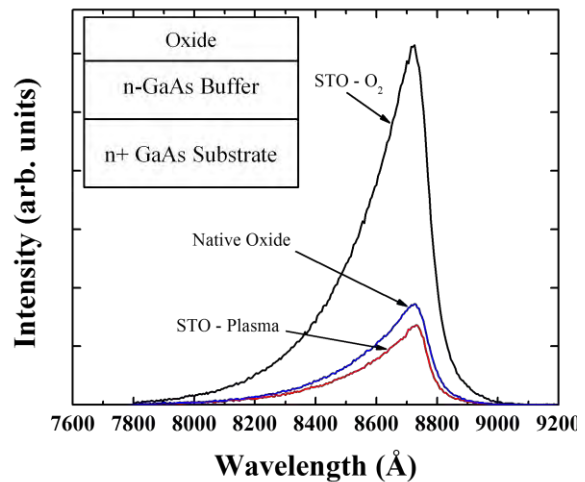


Figure 7: Room temperature photoluminescence spectra for the STO/GaAs structure. Also displayed is the spectrum for an identical GaAs structure that has been exposed to air forming a native oxide.

interfaces and the results used to screen materials for gate dielectric applications. As a reference an identical epitaxial structure was grown and exposed to air. The PL signal measured is a combination of the signal from the GaAs bulk, the substrate/GaAs epilayer interface and the GaAs epilayer/oxide interface. In this study the GaAs epilayer structure is identical for all the measured samples with the only difference being the top GaAs/oxide interface. As a result, differences in the PL intensity are related to the top oxide/GaAs interface. The GaAs/native

oxide interface represents the case for a pinned Fermi level due to states created in the bandgap once the clean GaAs is exposed to air [11]. Reduction of the defect density at this interface will result in an increase in the PL intensity. Figure 9 shows a comparison of the room temperature photoluminescence spectra from two STO/GaAs interfaces; one grown using molecular oxygen and the second with oxygen plasma during the bulk of the STO growth. Also shown is a similar GaAs structure which has been exposed to air. Since the GaAs substrate and bulk epitaxial layers are identical, and change in PL intensity will be due to defects at the top GaAs/oxide interface. The similarity in the PL intensity for the air-exposed GaAs surface and the STO/GaAs sample grown using oxygen plasma suggest comparable density of interfacial defects even though the STO layer is single crystal. The increase in the PL intensity from the structure grown using molecular oxygen is indicative of a decrease in the interfacial defect density. This result suggests some damage to the interface by the oxygen plasma creating a large density of optically active defects.

To investigate the interface bonding, a 20Å thick single crystal STO layer was first

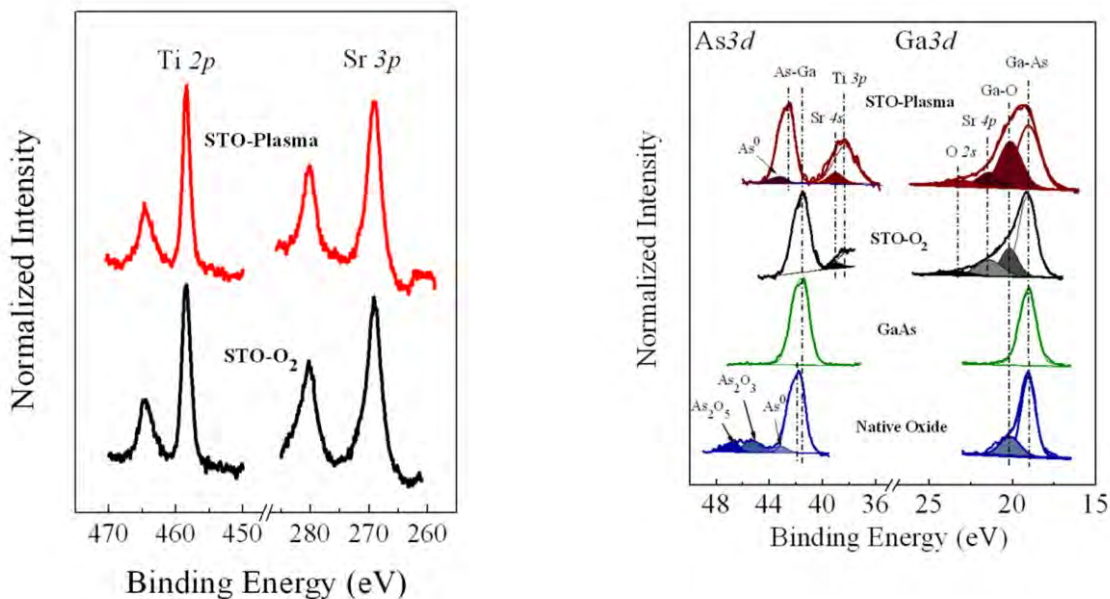


Figure 9: XPS spectra for the Ti 2p and the Sr 3d spectra for the STO layer grown using both oxygen plasma and molecular oxygen.

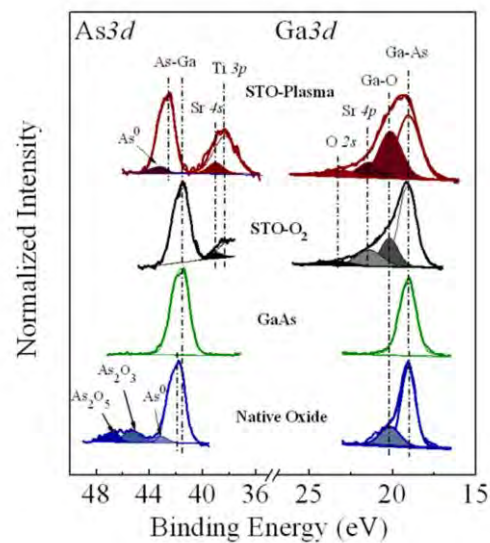


Figure 8: XPS spectra for the As 3d and Ga 3d spectra for a 20Å STO layer grown on GaAs (see text). For comparison the spectra are also shown for a clean GaAs surface and one on which a native oxide is form. The vertical lines are to aid in locating the relative peak positions.

grown on GaAs and the interface probed by XPS. This sample was then exposed to oxygen

plasma for a similar time/flux to that was used for the growth of the layer measured by PL in figure 9. Any change in bonding due to the diffusion of the active oxygen will be observed in the XPS measurements. Figure 10 shows the Sr 3p and Ti 2p XPS spectra for the STO films respectively in which there is little differences in the oxidation states for both elements. Complete oxidation of both Sr and Ti, even for the samples grown using molecular oxygen, attest to MBE as a viable growth technique for single crystal oxides. From the analysis of the XPS data no evidence of Ti-As bonding was detected at the oxide/semiconductor interface, even though a $\frac{1}{2}$ ML Ti prelayer was used prior to the nucleation of the STO buffer layer. It has been reported that the initial Ti prelayer reacted primarily with the surface As [8] prior to the STO growth but no investigations were carried out at the interface to determine the bonding configuration after the growth of the oxide layer. Based on TEM investigations of this interface, Klie et al. [12] found no evidence of the Ti. Instead they observed a sharp interface in which a SrO layer was in perfect registry with the As-terminated (1x1) substrate. It was speculated that a re-arrangement of the atoms at the interface during growth led to a more energetically favorable SrO layer next to the GaAs substrate [9] with some Ti diffusion into GaAs.

Figure 11 shows the spectra for Ga 3d and As 3d respectively for 4 samples. In addition to the 2 STO/GaAs structures the spectra are also shown for a clean GaAs surface and one that has been exposed to air. Clear differences can be seen in for both spectra with respect to the oxidation of Ga. The clean GaAs surface shows no Ga oxides as expected, while the other samples has varying amount of Ga oxides. The oxidation peak for Ga is much higher in the sample grown using oxygen plasma which is probably due to the reactive nature of atomic oxygen with interfacial Ga. It is known that during the growth of STO on Si oxygen readily diffuses through the oxide film and reacts with interfacial Si forming SiO₂ with thicknesses that increase with temperature and incident oxygen with even thicker SiO₂ layer that forms when oxygen plasma is used [13]. This is a possible mechanism in which the increase amount of Ga₂O₃ at the oxide/GaAs interface is caused by highly energetic oxygen atoms breaking the Ga-As bonds.

The spectra for As 3d shows no arsenic oxides for all the samples, except the GaAs surface that has been exposed to air, in agreement with the TEM investigation for the STO/GaAs interface that uses a Ti pre-layer [12]. It is well known that the GaAs native oxide consists of As

oxides in which the As exist in various oxidation states [14]. As expected the single peak for clean GaAs shows As bonded to Ga, the position of which can be used to represent an unpinned surface Fermi level. The position of the As 3d peaks are different for the 2 oxide layers grown on GaAs; the position for the layer grown using molecular oxygen is identical to that for the clean GaAs surface suggesting similar Fermi level positions within the bandgap, while the peak position for the layer grown using oxygen plasma has shifted to higher binding energy due to a large density of interfacial defects. The As 3d peak position for the air-exposed which has a pinned Fermi level has also shifted to higher binding energy but the shift is smaller as compared to the oxygen plasma grown STO layer indicating additional states at the interface. There is however As-As bonding present in the spectra of the As 3d feature for the sample in which the oxide layer was grown using an oxygen plasma. As can be seen in the Ga 3d spectra for this sample there is also an increased level of Ga 3+ bonding. This is possibly due to atomic oxygen diffusing through the oxide layer during growth breaking interfacial Ga-As bonds and combining with Ga. The free arsenic would then be free to combine with other arsenic forming clusters close to the interface.

2.4 CONCLUSIONS

Molecular beam epitaxy has been used to deposit single crystal SrTiO₃ on GaAs using both molecular and atomic oxygen generated using a plasma source. The interface quality has been probed using room temperature photoluminescence and *in-situ* x-ray photoelectron spectroscopy. X-ray diffraction measurements indicate that the oxide on single crystal when grown using both molecular and atomic oxygen with ½ monolayer Ti prelayer and molecular oxygen used for the initial nucleation on an As-stabilized c(4x4) GaAs surface. An increase in the GaAs PL intensity for the STO/GaAs structure grown using molecular oxygen suggest an interface with a reduce density of defects leading to some level of Fermi level unpinning. The density of interfacial defects is increased when oxygen plasma is used. In-situ photoemission measurements indicate that such an interface has an increase amount of oxidized Ga in the 3+ oxidation state with some level of As-As bonding.

References

- [1] R. A. McKee, F. J. Walker, M. F. Chisholm, *Phys. Rev. Letts.* 81 (1998) 1314-1317.
- [2] H. Li, X. Hu, Y. Wei, Z. Yu, X. Zhang, R. Droopad, A. A. Demkov, J. Edwards, K. Moore, W. Ooms, J. Kulik, and P. Fejes, *J. Appl. Phys.* 93, (2003) 4521
- [3] M. P. Warusawithana, C. Cen, C. R. Sleasman, J. C. Woicik, Y. Li, J. Klug, L. F. Kourkoutis, H. Li, L.-P. Wang, M. Bedzyk, D. A. Muller, L.-Q. Chen, J. Levy, D. G. Schlom, *Science* 324 (2009) 367
- [4] K. Nashimoto, D. K. Fork, T. H. Geballe, *Appl. Phys. Letts.* 60 (1992) 1199
- [5] E. J. Tarsa, M. De Graef, D. R. Clarke, A. C. Gossard, J. S. Speck, *J. Appl. Phys.* 73 (1993) 3276
- [6] M. Hong, Z. H. Lu, J. Kwo, A. R. Kortan, J. P. Mannaerts, J. J. Krajewski, *Science* 283 (1999) 1897
- [7] J.H. Yum, T. Akyol, M. Lei, D.A. Ferrer, Todd.W. Hudnall, M. Downer, C.W. Bielawski, G. Bersuker, J.C. Lee, S.K. Banerjee, *Thin Solid Films* 520 (2012) 3091
- [8] Y. Liang, J. Kulik, T. Eschrich, R. Droopad, Z. Yu, P. Maniar, *Appl. Phys. Letts* 85 (2004) 1217.
- [9] R. F. Klie, Y. Zhu, E. I. Altman, Y. Liang, *Appl. Phys. Letts.* 87 (2005) 143106
- [10] M. Passlack, in *Materials Fundamentals of Gate Dielectrics*, edited by A.A. Demkov and A. Navrotsky _Springer, New York, 2005_, pp. 403–467.
- [11] W. E. Spicer, I. Lindau, P. Skeath, C. Y. Su, P. Chye, *J. Vac. Sci. Technol.* 17 (1980) 1019-1027
- [12] Q. Qiao, R. F. Klie, S. Ogut, J. C. Idrobo, *Phys. Rev. B* 85 (2012) 165406
- [13] R. Droopad, Z. Yu, H. Li, Y. Liang, C. Overgaard, A. Demkov, X. Zhang, K. Moore, K. Eisenbeiser, M. Hu, J. Curless, J. Finder, *J. of Crystal Growth* 251 (2003) 638–644
- [14] T. Ishikawa, H. Ikoma, *Jpn. J. Appl. Phys.* [31](#) (1992) 3981-3987

Epitaxial Ferroelectric Oxides on Semiconductors- A route towards negative capacitance devices

ABSTRACT

Epitaxial ferroelectric BaTiO₃ layers were deposited on both Si and compound semiconductor substrates using molecular beam epitaxy. The films were grown using molecular oxygen and determined to be c-axis oriented as determined from x-ray diffraction measurements. High resolution transmission electron microscopy indicated the interface between the oxide and GaAs is free of structural defects while a thick layer of amorphous SiO₂ layer is present at the interface of the oxide and Si. Ferroelectric properties of the BaTiO₃ films were measured using piezoresponse force microscopy and spectroscopy. The BTO films show a piezoresponse amplitude ~5pm/V, and a coercive voltage of $V_c=1-2$ V with an as-grown polarization along the growth direction consistent with TEM observations.

3.1 INTRODUCTION

The need to reduce power in CMOS devices is critical to the evolution of the next generation devices as scaling continues. The use of new materials for the gate dielectric, and with the possibility of using III-V semiconductors in the channel, is creating new challenges to maintaining high on-off ratios. It has been predicted that the negative capacitance in using ferroelectric materials as part of the gate dielectric may be exploited to reduce subthreshold swing for ultra-low power MOSFET applications [1]. With a sub-60mV/decade switching behavior demonstrated in polymer ferroelectric MOSFET [2] and proof of concept capacitance enhancement in crystalline ferroelectric-dielectric bilayer [3], a pathway now exist for a MOS device incorporating ferroelectric gate materials. The challenge of using ferroelectric materials in such devices, especially oxides, includes the difficulty of integrating them epitaxially on semiconductors with the polarization in the required direction and heterointerfaces that would not degrade device performance. Successful integration of epitaxial oxides would also open up

the possibility of adding enhanced functionalities onto logic and high speed optoelectronic circuitry. In addition, using a ferroelectric gate dielectric, the carriers in the channel of a MOSFET device can be switched using the polarization of the gate dielectric leading to a single transistor non-volatile memory device.

Among the ferroelectric materials, BaTiO₃ (BTO) is well suited for integration with semiconductors. It is among the most widely studied material systems for its many properties that include piezoelectricity, ferroelectricity, pyroelectricity, and electro-optics relevant for a number of device applications [4-6] and as one layer of two-phase multiferroic systems [7, 8]. Most of the prior work on the growth of BTO on Si utilized a buffer layer between the film and the substrate with the reported films possessing in-plane polarization [9-11]. Vaithyanathan, *et al.* [12] used a relaxed Ba_xSr_{1-x}TiO₃ buffer layer to ensure c-axis orientation of the grown BTO layer. The authors suggest the buffer layer is needed to overcome the large lattice mismatch between the oxide and Si in addition to reducing the thermal strain upon cooling as a result of the differences on the coefficient of thermal mismatch. More recently c-axis oriented BTO films as determined by x-ray diffraction were grown on Si using a 5nm thick STO buffer layer [13] by MBE. However, these films exhibited no ferroelectric behavior which was thought to be due to insufficient oxygen during growth. Limited work was carried out on the growth of BTO on compound semiconductors using MBE. Most of the reported literature involved pulsed laser deposition of the oxide films on buffer layers such as MgO on GaAs. In 2003, Liang, *et al.* [14] have also demonstrated the growth of high quality STO on GaAs (100) with a crystalline transition across the GaAs/STO interface and a full width at half maximum (FWHM) of the STO (200) peak of 0.42° for a 100Å thick film. In this paper, the growth and properties of an epitaxial complex oxide that exhibit ferroelectricity on both Si and III-V heterostructures will be discussed.

2.2 EXPERIMENTAL

Oxide deposition was carried out on both 3 inch diameter Si and GaAs using a multi-chamber molecular beam epitaxy system. In the case for the growth on III-V substrates, an epitaxial layer of GaAs was first deposited in a solid source chamber dedicated for the growth of arsenic

containing compounds. After cooling in a flux of As, the epitaxial GaAs layer was then transferred via the UHV buffer to the oxide chamber ensuring a III-V surface that is free of any oxide. For the growth on silicon, substrate preparation was carried out in-situ using the Sr-deoxidation process to remove the native oxide and allow for the formation of the template layer as described in ref. [15]. Elemental sources and molecular oxygen were used for the growth of the oxide film. On both type of substrates a 2 unit cell SrTiO₃ nucleation layer was used as the buffer layer before the growth of the BaTiO₃ layer which was carried out at a substrate temperature of 500°C in an oxygen flux of 1×10^{-7} mbar. The STO nucleation on GaAs uses a $\frac{1}{2}$ ML Ti on a c(4x4) reconstructed surface using a process described in ref.[16]. No post growth annealing was used for the BTO film.

The surface crystallinity and stoichiometry of the oxide layer were monitored during growth using reflection high energy electron diffraction (RHEED), where the flux can be interrupted to ensure a Ba:Ti ratio of unity. The crystalline properties were determined using x-ray diffraction and TEM was used to investigate the microstructure, in particular the interface of the oxide with the semiconductor. Z-contrast images and EEL spectra shown in this study were acquired using the aberration-corrected JEOL ARM200CF, equipped with a 200 kV cold-field emission gun, post-column Gatan Enfina EELS spectrometer, and high-angle annular dark field and annular bright field detectors. A 22 *mrad* probe convergence semi-angle, a 90 *mrad* inner detector semi-angle for Z-contrast imaging were used in the experiments. The ferroelectric properties of the structures were investigated using piezoresponse force microscopy and spectroscopy.

2.3 RESULTS AND DISCUSSIONS

Unlike the present amorphous gate stack in current CMOS technology, ferroelectric gate materials need to be crystalline for the realization of polarization that is well oriented, preferably in the growth direction. BTO has a tetragonal (pseudo-cubic) crystal structure with an *a*- and *b*-axis lattice constant of 3.992 Å and *c*-axis lattice constant of 4.036 Å at room temperature. Thus, the lattice mismatch with GaAs is only 0.13% at room temperature and reduces to 0.08% at temperatures of around 500°C, the typical MBE growth temperature, when the BTO unit cell is rotated 45° on its (001) axis. Consequently under these conditions, it is expected that BaTiO₃

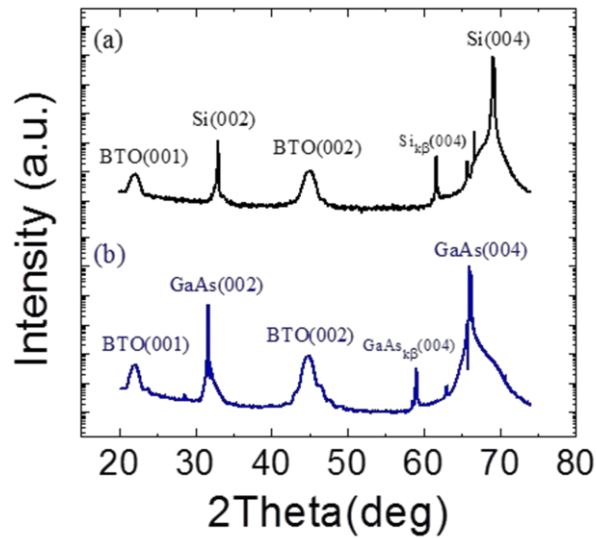


Figure 10: X-ray diffraction theta-2theta spectra for an 80Å thick epitaxial BaTiO₃ film on GaAs (top) and Si (bottom).

rotation of the oxide films with respect to the semiconductor substrates. While the lattice matched is negligible when grown on GaAs, there is a 4.0% mismatch when BTO is grown on Si and with the STO buffer layer expected to be commensurately strained, and with a critical thickness at growth temperature expected to be around 10Å, there will be complete relaxation of the BTO film for the thickness measured. The identical positions of the XRD peaks for both GaAs and Si do indeed suggest that there is complete relaxation of the oxide films on when grown on a Si substrate resulting in a c-axis oriented in the growth direction even using a strained 2 unit cell STO buffer layer. This is in contrast to Viathanathan *et. al.* [12] who suggested that a thick relaxed buffer layer is needed for achieving c-axis oriented BTO films on Si. Figure 13 shows the RHEED patterns after the growth of the BTO film on Si and GaAs with the intensity modulations along the streaks of the patterns for growth on Si suggest relaxation of the epitaxial layer.

will be grown on GaAs with its c-axis aligned in the growth direction. Figure 12 show the θ -2 θ scan of an approximately 80Å thick BTO layer on both GaAs and silicon. The peaks present confirmed that the oxide layer is (100) oriented and the out-of-plane lattice constant for BTO was determined to be 4.032Å clearly demonstrating that the BTO layers were grown with the c-axis oriented along the growth direction on both type of substrates. Pole figures for both samples confirmed the 45° degree

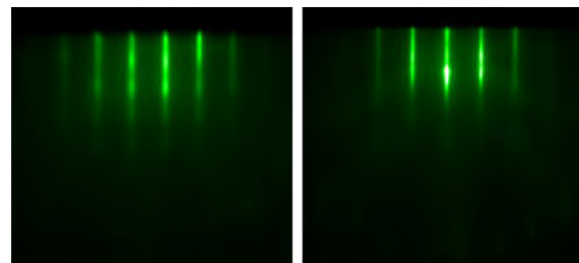


Figure 11: RHEED images taken after the grown of 80Å thick BTO film on Si (left) and GaAs (right) along the [110] azimuth. The modulation in the streaks for the layer grown on Si suggest some level of disorder and roughness due to the relaxation of the BTO layer due to the lattice mismatch.

The microstructure of the BTO films was investigated using scanning transmission electron microscopy. Figure 14 shows the X-contrast images for a BTO film deposited epitaxially on both Si and GaAs. The BTO/GaAs interface exhibits a crystalline transition with perfect registry to the substrate. The BTO/Si interface exhibits a crystalline transition with perfect registry to the substrate. The 2 unit cell STO buffer layer can be seen in the STEM for the BTO film on

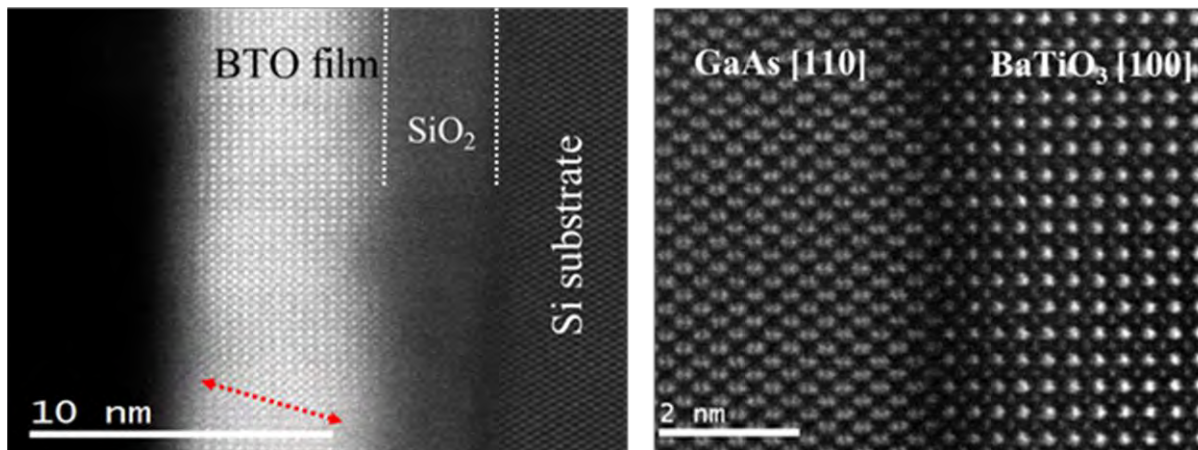


Figure 12: Atomic-resolution Z-contrast images of BaTiO₃ grown on Si (left) and GaAs (right). The images were taken along the (110) projection.

GaAs with the interface free from any oxides attesting to the stability of the STO/GaAs interface during growth. In fact, photoemission measurements have detected the presence of Ga-O bonds at the oxide/GaAs interfaces with no evidence of As oxides [16]. The structure with the oxide grown on silicon substrate displays a thick layer of amorphous SiO₂. This is due to the tendency of oxygen to diffuse through the oxide film during growth and react with interfacial Si. The thickness of this layer can be controlled using the temperature, oxygen partial pressure and oxygen species (atomic oxygen would result in a thicker SiO₂ layer compared to molecular oxygen). While this layer may be problematic for some device applications, it can be the ideal gate dielectric stack in CMOS devices in combination with the ferroelectric BTO layer. The STEM image also reveals grain boundaries (indicated by the arrow) and defects in the STO film as a result of relaxation due to the 4% lattice mismatch.

The ferroelectric properties of the films were determined using piezoresponse force microscopy (PFM), a technique used to image and manipulate ferroelectric domains [17]. The polarization of the ferroelectric domains is locally switched by applying a DC bias V_{dc} above the coercive voltage, allowing domain patterning when mapping V_{dc} onto the tip position during scanning. Figure 15 shows dual-frequency PFM characterization of the BTO/GaAs and BTO/Si surface

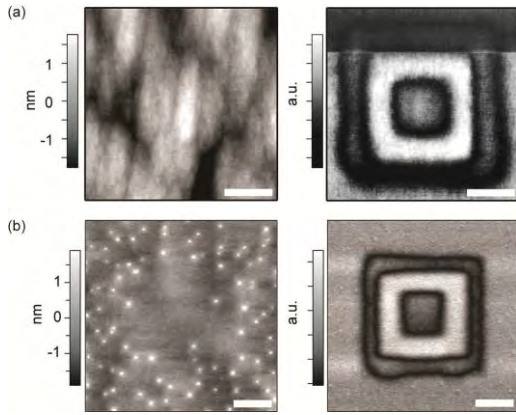


Figure 13: Height (left) and PFM amplitude (right) from BTO on GaAs (a) and BTO on Si (b), acquired simultaneously after patterning a $3 \mu\text{m} \times 3 \mu\text{m}$ square ring by applying $\pm 5 \text{ V}$ DC bias (Scale bars: $1 \mu\text{m}$; $V_{\text{ac}}=2 \text{ V}$). The inner ring in the amplitude images (right) corresponds to where -5 V sample bias was applied, while the outer ring and center square correspond to where $+5 \text{ V}$ was applied. V_{ac} is the PFM driving voltage for both excitation frequencies.

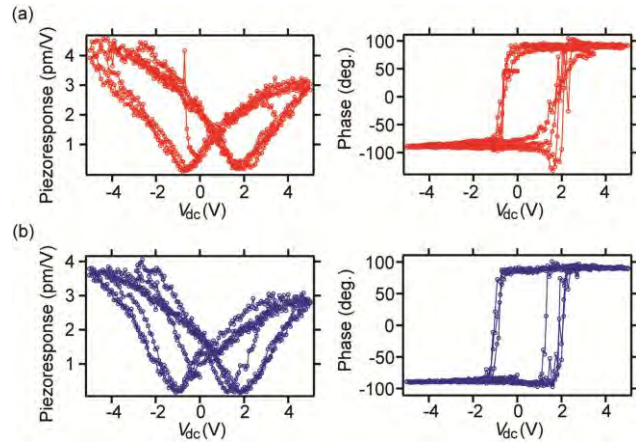


Figure 16: Piezoresponse force spectroscopy hysteresis curves for piezoresponse amplitude (left) and phase (right) for BTO on GaAs (a) and BTO on Si (b). Driving voltages were (a) $V_{\text{ac}}=2 \text{ V}$ and (b) $V_{\text{ac}}=1 \text{ V}$ (at dual-frequencies).

after ferroelectric domain patterning of a square ring. The center square and outer ring were patterned with $V_{\text{dc}}=-5 \text{ V}$, while the inner ring was patterned with $V_{\text{dc}}=+5 \text{ V}$. Simultaneous height and piezoresponse scans show that the imaged pattern is due entirely to the piezoresponse and not cross-coupling to the surface topography. Piezoresponse force spectroscopy amplitude and phase hysteresis curves (figure 16) indicate that the polarization is repeatedly switchable. Ferroelectricity is confirmed by a 180 degree phase difference in the piezoresponse of oppositely polarized domains. The BTO shows a piezoresponse amplitude $\sim 5 \text{ pm/V}$, and a coercive voltage of $V_c=1-2 \text{ V}$, with respect to the sample, which was grounded. Similar patterning and characterization were repeated several times on different areas of the sample with similar results. Moreover, the result also indicated that the as-deposited BTO is polarized on both Si and GaAs substrates, consistent with X-ray diffraction data showing the c-axis aligned out-of-plane. Additional evidence for this remnant polarization is the displacement of the Ti atoms observed in the high resolution TEM of figure 14 leading to polarization that is directed along the growth direction.

2.4 CONCLUSIONS

High quality crystalline BaTiO₃ layers have been deposited on both Si and GaAs using molecular beam epitaxy. The as grown layers were determined to be fully relaxed on Si and commensurate with GaAs that has an extremely small lattice mismatch with BTO. X-ray diffraction determined that the oxide layers were grown with the c-axis oriented in the growth direction with the oxide layer completely relaxed on Si and grown commensurate on GaAs which has a negligible lattice mismatch with BTO. The interface of between the oxide and GaAs appears to be free of any structural defects from TEM observations while an amorphous layer of SiO₂ is present at the interface with silicon. On both substrates the oxide layer was found to be ferroelectric with piezoresponse amplitude ~5pm/V, and a coercive voltage of $V_c=1-2$ V. The as-grown layers possess polarization along the growth direction due to the displacement of Ti atoms as observed in TEM studies.

References

- [1] S. Salahuddin and S. Datta, "Can the subthreshold swing in a classical FET be lowered below 60mV/decade?," *IEEE International Electron Devices Meeting 2008*, pp. 693-696, 2008.
- [2] A. Rusu, G. A. Salvatore, D. Jimenez, and A. M. Ionescu, "Metal-Ferroelectric-Meta-Oxide-semiconductor field effect transistor with sub-60mV/decade subthreshold swing and internal voltage amplification " *IEEE International Electron Devices Meeting 2010* pp. 395-398, 2010.
- [3] A. I. Khan, D. Bhowmik, P. Yu, S. J. Kim, X. Pan, R. Ramesh, and S. Salahuddin, "Experimental evidence of ferroelectric negative capacitance in nanoscale heterostructures," *Applied Physics Letters*, vol. 99, Sep 12 2011.
- [4] J. H. Li, Z. F. Liu, B. W. Wessels, Y. M. Tu, S. T. Ho, A. Joshi-Imre, and L. E. Ocola, "Hexagonal photonic crystal waveguide based on barium titanate thin films," in *Optical Components and Materials Viii.* vol. 7934, M. J. F. Digonnet, *et al.*, Eds., ed, 2011.
- [5] J. F. Scott, "Applications of modern ferroelectrics," *Science*, vol. 315, pp. 954-959, Feb 2007.
- [6] R. Waser, *Nanoelectronics and Information Technology*: Wiley, 2003.
- [7] S. Sahoo, S. Polisetty, C. G. Duan, S. S. Jaswal, E. Y. Tsymbal, and C. Binek, "Ferroelectric control of magnetism in BaTiO₃/Fe heterostructures via interface strain coupling," *Physical Review B*, vol. 76, Sep 2007.
- [8] M. K. Lee, T. K. Nath, C. B. Eom, M. C. Smoak, and F. Tsui, "Strain modification of epitaxial perovskite oxide thin films using structural transitions of ferroelectric BaTiO₃ substrate," *Applied Physics Letters*, vol. 77, pp. 3547-3549, Nov 2000.
- [9] D. K. Fork, F. A. Ponce, J. C. Tramontana, and T. H. Geballe, "Epitaxial MgO on Si(001) for Y-Ba-Cu-O thin-film growth by pulsed laser deposition," *Applied Physics Letters*, vol. 58, pp. 2294-2296, May 1991.
- [10] R. A. McKee, F. J. Walker, J. R. Conner, E. D. Specht, and D. E. Zelmon, "Molecular-beam epitaxy growth of epitaxial barium silicide, barium oxide, and barium-titanate on silicon," *Applied Physics Letters*, vol. 59, pp. 782-784, Aug 1991.

- [11] Z. Yu, J. Ramdani, J. A. Curless, J. M. Finder, C. D. Overgaard, R. Droopad, K. W. Eisenbeiser, J. A. Hallmark, W. J. Ooms, J. R. Conner, and V. S. Kaushik, "Epitaxial perovskite thin films grown on silicon by molecular beam epitaxy," *Journal of Vacuum Science & Technology B*, vol. 18, pp. 1653-1657, May-Jun 2000.
- [12] V. Vaithyanathan, J. Lettieri, W. Tian, A. Sharan, A. Vasudevarao, Y. L. Li, A. Kochhar, H. Ma, J. Levy, P. Zschack, J. C. Woicik, L. Q. Chen, V. Gopalan, and D. G. Schlom, "c-axis oriented epitaxial BaTiO₃ films on (001) Si," *Journal of Applied Physics*, vol. 100, 2006.
- [13] G. Niu, S. Yin, G. Saint-Girons, B. Gautier, P. Lecoeur, V. Pillard, G. Hollinger, and B. Vilquin, "Epitaxy of BaTiO₃ thin film on Si(001) using a SrTiO₃ buffer layer for non-volatile memory application," *Microelectronic Engineering*, vol. 88, pp. 1232-1235, Jul 2011.
- [14] Y. Liang, J. Kulik, T. C. Eschrich, R. Droopad, Z. Yu, and P. Maniar, "Hetero-epitaxy of perovskite oxides on GaAs(001) by molecular beam epitaxy," *Applied Physics Letters*, vol. 85, pp. 1217-1219, Aug 16 2004.
- [15] W. Yi, X. M. Hu, L. Yong, D. C. Jordan, B. Craigo, R. Droopad, Z. Yu, A. Demkov, J. L. Edwards, K. Moore, and W. J. Ooms, "Si(100) surface cleaning using Sr and SrO," *Silicon Materials-Processing, Characterization and Reliability*, vol. 716, pp. 139-144, 2002.
- [16] R. Contreras-Guerrero, M. Edirisooriya, O. Noriega, and R. Droopad, "Interface properties of MBE grown epitaxial oxides on GaAs," *Journal of Crystal Growth*, 2013.
- [17] S. V. Kalinin, A. N. Morozovska, L. Q. Chen, and B. J. Rodriguez, "Local polarization dynamics in ferroelectric materials," *Reports on Progress in Physics*, vol. 73, May 2010.

Structural Properties of SrTiO₃ on GaAs(001) Interface

ABSTRACT

The successful epitaxial growth of SrTiO₃ on Si and GaAs showed that it is possible to integrate the functional oxides with semiconductors incorporating unique multifunctional properties of oxides into various existing semiconductor technologies. While SrTiO₃ has been also deposited on GaAs without amorphous interfacial layers, the exact interface structure has been controversial; on one hand, scanning Transmission Electron Microscopy (STEM) shows As atoms at the interface. X-ray photoelectron spectroscopy (XPS) measurements, on the other hand, do not show peaks associated with As-O bonding, indicating that the GaAs/STO interface does not involve an As/oxide layer, contradicting initial STEM observations. Using *ab initio* calculations, we determine the interfacial structure of a SrTiO₃ film on a GaAs substrate to help clarify the apparently discrepancy between the XPS and the STEM measurements. The calculations reveal that, under the condition that allows atomically abrupt interfaces, the energetically most stable interface is As/Sr/TiO₂ structure, in accordance with both XPS and STEM measurements.

4.1 INTRODUCTION

Compound semiconductors form the basis for a large number of high-speed optoelectronic devices that are being used in optical communications and power amplifiers in wireless mobile devices. In addition, they are currently being considered as channel materials in future generations of low-power Si CMOS devices to overcome the limitations of Si performance that results from device scaling. Crystalline oxides on the other hand, have unique multifunctional properties that can be exploited for devices that utilize various ferroic properties such as ferroelectricity and ferromagnetism. When combined with compound semiconductors, oxides can be used for various reconfigurable spin-based optoelectronic devices where, for example, the polarization of a ferroelectric layer is used to switch two-dimensional electron gas on and off in a compound semiconductor heterostructure and/or to inject spin into heterojunction optical emitters. These devices can only be realized if the oxides are epitaxially deposited on compound semiconductor, producing interfaces that have low interface state density. Therefore, an

understanding of the growth and interface properties is imperative for the heterointegration of these dissimilar material systems. In particular, the atomic structure of the oxide/semiconductor interface is necessary to tailor the properties for device applications.

With the successful growth of epitaxial SrTiO₃ (STO) on Si using Molecular Beam Epitaxy (MBE) [1], it is possible to monolithically integrate the rich properties of oxides, high carrier mobility and optical properties of compound semiconductors, and the mature Si technology to create a new class of hybrid devices. Among the first reported oxide deposited on GaAs was carried out using laser MBE and involved the growth of MgO on various terminated GaAs surfaces [2]. However, the resultant films consisted of textures and columnar grains. Hong and co-workers [3] used electron beam evaporation to deposit cubic gadolinium oxide as a gate dielectric on GaAs and demonstrated both inversion and accumulation in the diode structures using capacitance-voltage measurements. More recently, Atomic Layer Deposition technique was used to grow crystalline BeO thin films on both Si and GaAs [4] for high-k dielectric applications. X-ray diffraction (XRD) showed that different crystal structures of BeO exist in these ALD grown films. MBE was used to successfully deposit STO on GaAs without any amorphous interfacial layer [5]. By analyzing the STO/GaAs interface with X-ray photoemission spectroscopy (XPS) and scanning transmission electron microscopy (STEM), Klie *et al.* concluded that the pinning of Fermi level is determined by the interface structure [6]; the Fermi level is pinned when STO is grown directly on GaAs and unpinned when a Ti template is used. Thin layers of STO grown on GaAs were used as buffer layers to deposit BaTiO₃ layers [7]. While oxides such as STO can be grown epitaxially on GaAs with a two-dimensional nucleation, the reverse is not always possible. The nucleation of GaAs on STO results in three-dimensional island growth, leading to a large number of defects at the interface [8]. Understanding the interface structure between oxides and GaAs can help to tailor a growth process in which compound semiconductors can nucleate 2D on crystalline oxide surface. The experimental (computed) lattice parameters of GaAs bulk and SrTiO₃ bulk are $a_{\text{GaAs}}=5.653$ (5.76) Å and $a_{\text{SrTiO}_3}=3.905$ (3.95) Å. Due to the large lattice mismatch between them, epitaxial SrTiO₃ (STO) layers had to be grown on GaAs(001) with the primitive vectors in the plane parallel to interface rotated by 45° with respect to the GaAs unit cell ($a_{\text{layer}} = a_{\text{SrTiO}_3}\sqrt{2} = 5.523$ (5.586) Å). The experimental (computed) lattice parameter's mismatch, $\epsilon = (a_{\text{GaAs}} - a_{\text{layer}}) / a_{\text{GaAs}}$, can be reduced from ~30% to 2.3% (3.0%) .

In this study, we investigate the atomic structure of the STO/GaAs interface through in-situ XPS and high-resolution cross-section STEM. These measurements are compared with *ab initio* Density Functional Theory (DFT) calculations to illuminate the underlying energetics of the interface structure. The results of such understanding will guide the growers in surface modifications to alter the surface energetics.

4.2. EXPERIMENTS

For a successful deposition of crystalline oxide film on semiconductor substrates, it is necessary to maintain high vacuum to prevent the oxidation of the semiconductor surface in the presence of oxygen. In addition the use of reactive atomic oxygen species produced from a plasma source can seriously damage the surface/interface during the initial stages of oxide film growth. We used a deposition system that consists of an oxide growth chamber, a III-V growth chamber, and a photoelectron spectroscopy analysis chamber for deposition and analysis at all stages of the growth process. This system configuration allows the wafers to be transferred into the various chambers without exposure to atmosphere. It ensures that the surface remains clean and well-ordered for subsequent deposition and eliminates artifacts during spectroscopic analysis that can result from atmospheric contamination. Growth rates are determined using the reflection high-energy electron diffraction (RHEED) oscillation technique and the substrate temperature is measured using an optical pyrometer that is cross-referenced using a KSA bandit system and transitions of surface reconstructions. The oxide growth is carried out using elemental Sr and Ti from effusion cells and high purity molecular oxygen. Oxide stoichiometry and surface structures were monitored *in situ* using RHEED.

GaAs layers are grown using elemental sources at a substrate temperature of 580°C and a growth rate of 0.8 MLs/sec after which the wafers are cooled under an As flux until the temperature is <300°C at which time the As cracker valve is closed. The substrate is then transferred into the oxide chamber where the substrate temperature is increased to around 300°C to achieve a GaAs c(4x4) surface reconstruction. A ½ ML Ti prelayer is deposited prior to the nucleation of the oxide layer which comprised of co-deposition of Sr, Ti and molecular oxygen at the substrate temperature of 300°C for a total thickness of 1-2 unit cells. This is followed by an annealing at 500°C for 3 minutes after which co-deposition of STO is continued until the desired thickness is achieved. RHEED is used throughout the growth to ensure stoichiometric oxide growth.

The oxidation states and chemical bonding at the interface are probed using XPS in the analysis chamber that incorporates a Scienta SES 2002 hemispherical analyzer and a dual anode x-ray source. The structural properties of the films are characterized *ex situ* using XRD while the surface morphology is mapped using AFM with a Si probe tip.

4.3. CALCULATION

The atomic structure and the total energy of the interfaces are calculated within the Density Functional Theory (DFT) using the Vienna *ab initio* Simulation Package (VASP) [9]. The generalized gradient approximation (DFT-GGA) [10] is used for exchange-correlation potential. The electronic wave-functions are describe by a projector augmented wave (PAW) method [11] with an energy cutoff of 500 eV. The Ga *d* and Ti *p* electrons are treated explicitly as valence electrons. For slab calculations and bulk calculations, the Brillouin zone is sampled with 4×4×2 and 8×8×8 Monkhorst-Pack k-point grid [12], respectively. The slab calculations include at least 10Å vacuum so that the spurious image interactions in the film growth direction is negligible. All atom positions in the interface structures are fully relaxed until the force on each atom becomes less than 4.0×10⁻⁵ eV/Å and the total energy converges within 10⁻⁴ eV. The theoretical lattice constant, 5.76 Å, is used for the GaAs substrate. We computed the Gibbs free energies of 32 interfaces with different terminations, e.g., TiO₂/As, TiO₂/Ga, SrO/As, SrO/Ga, Ti/As, Ti/Ga, Sr/As and Sr/Ga. In total of 160 different structures are computed to determine the most stable interface structure.

The thermodynamic stability of the interface structures is calculated using the Gibbs free energy defined as:

$$G = E_{interface} - n_{Sr}\mu_{Sr} - n_{Ti}\mu_{Ti} - n_O\mu_O - n_{Ga}\mu_{Ga} - n_{As}\mu_{As} , \quad (1)$$

where n_X and μ_X represent the number of atoms and the chemical potential of the element X, respectively. $E_{interface}$ is the DFT total energy of the interface structure. The chemical potentials in Eq. (1) are constrained by the chemical potential of the bulk SrTiO₃, i.e., $\mu_{Sr} + \mu_{Ti} + 3\mu_O = \mu_{STO}$, and the bulk GaAs, i.e., $\mu_{Ga} + \mu_{As} = \mu_{GaAs}$. The chemical potentials μ_{Sr} , μ_{Ti} , and μ_O are further constrained to prevent formation of other binary and ternary structures, as obtained by C. S. Hellberg *et al* [13].

4.4. RESULTS AND DISCUSSIONS

The GaAs surface reconstruction results from the dimerization of the As dangling bonds and depends on the excess As on the surface. Deposition of other adatoms disrupts the bonding, resulting in a change of the surface reconstructions with transfer of electron between the surface adatoms. Figure 17 shows the GaAs c(4x4) reconstruction (Fig 1a) and the resulting reconstruction when a ½ ML Ti (Fig 1b) and ½ ML Sr (Fig 1c) is deposited on GaAs c(4x4). During this study, the Ti prelayer is used for the nucleation and growth of STO on GaAs. Deposition of the Ti atoms creates a sub

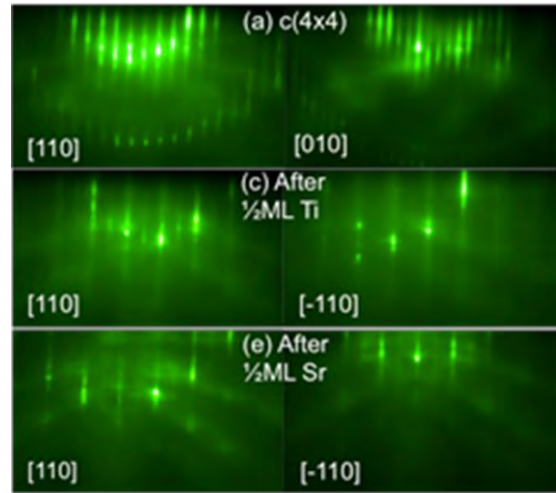


Figure 16. RHEED images showing the modification of the (a) GaAs c(4x4) surface reconstruction when (b) Ti prelayer and (c) Sr prelayer is deposited at 300C

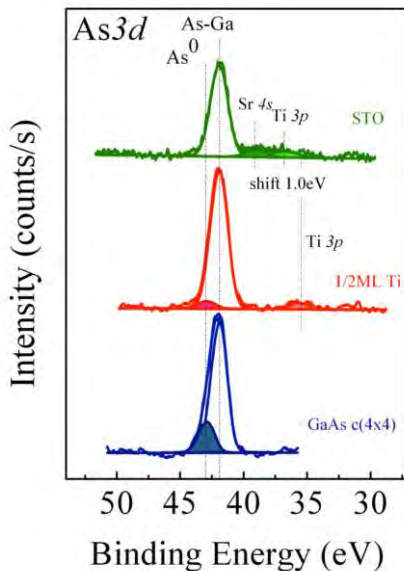


Figure 158: XPS spectra of the As 3d peak for (a) a GaAs c(4x4) reconstructed surface, (b) after the addition of ½ ML Ti and (c) after the growth of approximately 20A STO on GaAs.

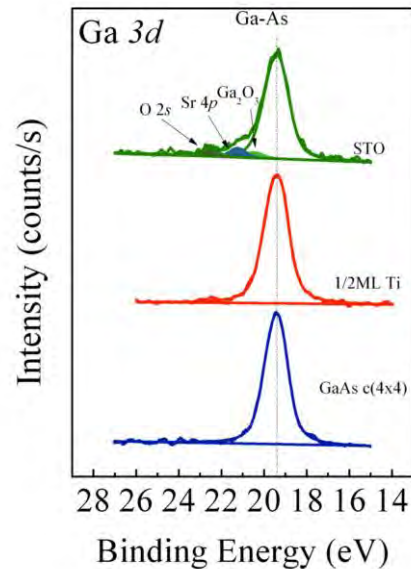


Figure 149: XPS spectra for the Ga 3d peak for (a) a GaAs c(4x4) reconstructed surface, (b) after the addition of ½ ML Ti and (c) after the growth of approximately 20A STO on GaAs.

monolayer of Ti-As bonding as evidence in the XPS spectra of Figure 18. The As 3d spectrum

for the c(4x4) reconstructed surface shows a peak that is the convolution of 2 peaks resulting from As bonded to Ga and As bonded to As. The As-As bonding is expected since the c(4x4) GaAs surface has an excess of As. Deposition of the Ti on this surface results in Ti-As bonding which shows up in the peak with binding energy of 36 eV resulting in a reduction of the As-As bonding. A closer examination of figure 2 shows that once the STO layer is formed there is no evidence of Ti-As bonding as the Ti peak has shifted to higher binding energy that would be expected for a 4+ oxidation. Figure 19 shows the spectra for the Ga 3d peak that will be a convolution of the Ga bonding in the bulk GaAs and at the semiconductor/oxide interface. The addition of Ti to the GaAs surface has no effect on the peak position of the Ga electronic configuration implying that the Ga atoms at the interface remain undisturbed. On the other hand, some evidence of Ga oxides is present after the growth of the STO layer with Ga in its 3+ oxidation state.

Aberration-corrected scanning transmission electron microscopy (STEM), in particular high-angle annular dark field (HAADF) imaging is used to investigate the structural properties of the STO/GaAs interface. More specifically, the JEOL ARM200CF at the University of Illinois at Chicago, which is equipped with a cold-field emission electron gun, a GATAN Enfina post-column electron energy-loss spectrometer and several annular dark field detectors, provided atomic-resolution HAADF images of the STO/GaAs (see Figure 20), where the recorded image intensity is proportional to the average atomic number. It was previously shown that the STO film is sensitive to a 200 keV electron beam. Therefore the image shown in Figure 20 was taken with a primary beam energy of 80 keV. The HAADF image in Figure 4 clearly demonstrates that the GaAs substrate is terminated by As, which is in direct contact with the Sr-O layer. In agreement with earlier reports, we do not find any Ti at the STO/GaAs interface, despite the deposition of the $\frac{1}{2}$ ML of the Ti prelayer. Moreover, previous electron energy-loss spectroscopy measurements [14] have demonstrated that the STO near the GaAs interface is highly oxygen deficient.

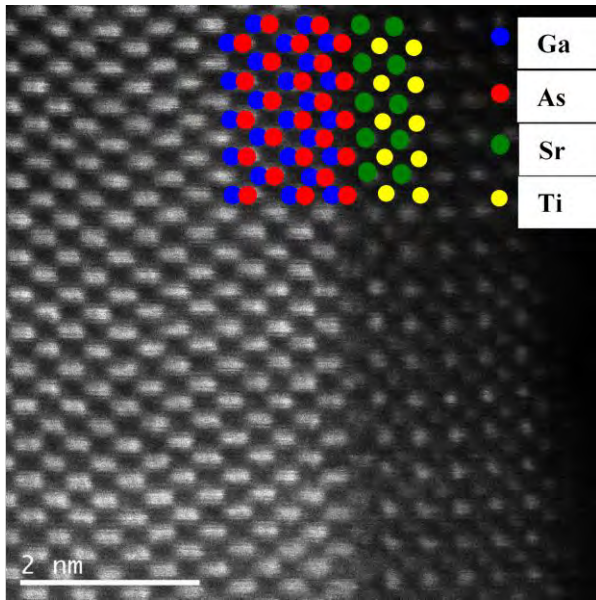


Figure 18: Atomic-resolution HAADF image of 4 monolayers SrTiO₃ on As-terminated GaAs. The SrTiO₃ film is seen in the [100] and the GaAs in the [110] projection.

To help clarify the discrepancy between the XPS and the STEM measurements and to determine the atomic structure of STO/GaAs interface, we perform *ab initio* DFT calculations. We calculate both Ga and As substrate surfaces interfaced with either SrO or TiO₂ surface layer. We also include Sr and Ti intermediate layers (ILs) between STO and GaAs surfaces, to account for the high concentration of oxygen vacancies at the interface, suggested by our previous STEM results. A Sr and Ti IL can be considered oxygen depleted SrO and TiO₂ layers, respectively.

The calculated Sr concentration, x , in the IL is varied in the range $x=(1/8, 1)$ in an increment of $1/8$. The STO films of 1 to 5 monolayers (MLs) thickness are computed.

The calculated Sr concentration, x , in the IL

The minimum Gibbs free energies of different interface structures, shown in Figure 21, reveal that the most energetically stable interface structure is As/Sr/TiO₂ structure, regardless of the STO film thickness. The Ti IL also makes the interface more stable compared with TiO₂ interface layer. The stability of the interface with metal intermediate layer is attributed to the fact that the oxygen vacancies are stable at the interface [15]. The relative stability of metal IL over oxide layer does not depend on the semiconductor surface, whether the semiconductor is terminated with As or Ga. Between the As- and Ga-terminated surfaces, Figure 21 shows that the formation energy of the As-terminated

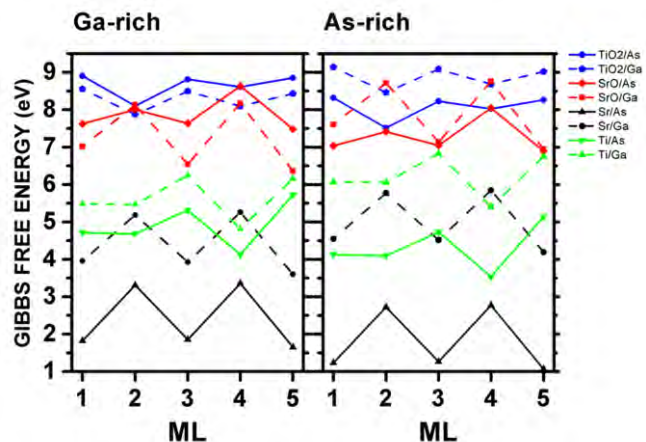


Figure 17: The minimum Gibbs free energies of STO films on a GaAs substrate. The legends represent the first molecular layer of the STO and the top layer of GaAs. In case of Sr intermediate layer interface, i.e. Sr/Ga and Sr/As, TiO₂ layer is deposited on Sr IL.

surface is much lower than that of the Ga-terminated surface. The atomic configuration of the lowest energy interface structures of 1, 2, 3, and 4 ML thick SrTiO₃ films on GaAs [001] are shown in Figure 22 (b) - (e). The Sr atoms in the intermediate layer are located above the middle of the sides of the GaAs [001] unit cell with As surface atoms located at $a_{\text{GaAs}}(0, 0, 0)$ and $a_{\text{GaAs}}(\frac{1}{2}, \frac{1}{2}, 0)$, as depicted in Figure 22 (k). The interlayer distances between the As surface and the Sr IL in Figure 22 (a) - (e) are 1.06, 1.33, 1.24, 1.35, and 1.31 Å. The As-Sr bond length in (a) - (e) interfaces are 3.07, 3.17, 3.13, 3.18, and 3.17 Å.

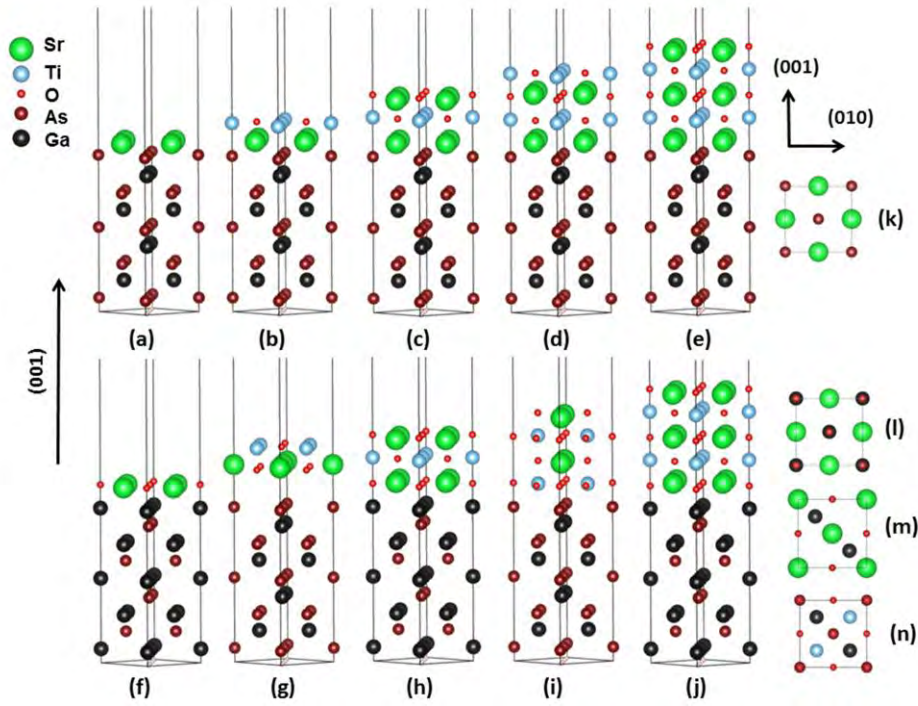


Figure 19: The atomic configuration of the most stable SrTiO₃ films on GaAs (001). (a)-(e) show the structures that are energetically most stable for each film thickness. They all have a Sr-only intermediate layer between As and TiO₂ surfaces. (k) shows the overview of the atomic arrangement of As/Sr interface. (f)-(j) show the most stable interface structures with oxidized STO surface layers. (k) displays the overview of the atomic arrangement of the Ga/SrO interfaces in (a)-(e). The overview of interfaces in (f), (h) and (j) are shown in (l). (m) and (n) show the overview of the interface layers in (g) and (i), respectively.

In case of interfaces without Sr IL, the relative stability of the interfaces varies depending on the film thickness. For non-stoichiometric films, i.e., odd number of STO MLs, the Ga/SrO interface has the lowest formation energy. The oxygen atoms sit on top of Ga atoms, forming strong Ga-O bonds, as depicted in Figure 22 (l). For stoichiometric films, on the other hand, the formation energies of different surfaces are very close, as shown in Figure 21. As the STO film thickness grows, the Ga/SrO interface becomes more stable than other interfaces.

In comparison with experiment, the lowest formation energy interface structure agrees with the STEM and EELS measurements. Because the oxygen flux is limited to 10^{-8} mbar during the growth of the first STO unit cell and also because the oxygen vacancies at the interface have lower formation energy, the interface is stuck with oxygen depleted state, rather than allowing the oxygen atoms to diffuse into the interface. The XPS measurement, on the other hand, is indicative to the presence of oxidized GaAs surface. In the area where the oxygen is relatively abundant, the Ga/SrO interface can form. The partially oxidized surface area, however, should be smaller than oxygen depleted area because of As treatment on the substrate as well as low oxygen pressure. The GaAs surface reconstruction has little influence on the growth of crystalline STO films. We find that the dimerization of surface As atoms does not necessarily stabilize the interface, in contrast to Si/STO interfaces [16]. The difference in the interface formation energy between the (2x1) As surface and regular As surface is less than 0.025 eV per unit cell area.

4.5. CONCLUSIONS

Through a combined analysis of *ab initio* calculations, XPS, and STEM measurements, we obtained a comprehensive understanding of the interface atomic structure and the correlation between the interface structure and the growth condition. The low oxygen pressure during the first layers of STO and the stability of oxygen depleted interface structure conspire the As/Sr/TiO₂ structure at the GaAs/STO interface.

References

- [1] H. Li, X. Hu, Y. Wei, Z. Yu, X. Zhang, R. Droopad, A. A. Demkov, J. Edwards, K. Moore, W. Ooms, J. Kulik, and P. Fejes, *Journal Of Applied Physics* **93** (8), 4521 (2003); R A McKee, F J Walker, and M F Chisholm, in *Phys. Rev. Lett.* (American Physical Society, 1998), Vol. 81, pp. 3014; Maitri P. Warusawithana, Cheng Cen, Charles R. Sleasman, Joseph C. Woicik, Yulan Li, Lena Fitting Kourkoutis, Jeffrey A. Klug, Hao Li, Philip Ryan, Li-Peng Wang, Michael Bedzyk, David A. Muller, Long-Qing Chen, Jeremy Levy, and Darrell G. Schlom, *Science* **324** (5925), 367 (2009).
- [2] E. J. Tarsa, M. De Graef, D. R. Clarke, A. C. Gossard, and J. S. Speck, *Journal Of Applied Physics* **73** (7), 3276 (1993); Keiichi Nashimoto, David K. Fork, and Theodore H. Geballe, *Appl Phys Lett* **60** (10), 1199 (1992).
- [3] M. Hong, J. Kwo, A. R. Kortan, J. P. Mannaerts, and A. M. Sergent, *Science* **283** (5409), 1897 (1999).
- [4] J. H. Yum, T. Akyol, M. Lei, D. A. Ferrer, Todd W. Hudnall, M. Downer, C. W. Bielawski, G. Bersuker, J. C. Lee, and S. K. Banerjee, *Thin Solid Films* **520** (7), 3091 (2012).
- [5] Y Liang, J Kulik, TC Eschrich, R Droopad, Z Yu, and P Maniar, *Appl Phys Lett* (2004), Vol. 85, pp. 1217.
- [6] RF Klie, Y Zhu, EI Altman, and Y Liang, *Appl Phys Lett* (2005), Vol. 87, p. 143106.
- [7] R. Contreras-Guerrero, J. P. Veazey, J. Levy, R. Droopad, *Appl Phys Lett* 102 (2013) 012907
- [8] R. Droopad, J. Curless, Z. Yu, D. Jordan, Y. Liang, C. Overgaard, H. Li, T. Eschrich, J. Ramdani, L. Hilt, B. Craigo, K. Eisenbeiser, J. Kulik, P. Feyes, J. Finder, X. Hu, Y. Wei, J. Edwards, K. Moore, M. O'Steen, O. Baklenov, *Inst. Phys. Conf, Ser. No 174 p. 1-8* (2003)
- [9] G Kresse and J Furthm ulla, in *Phys. Rev. B* (American Physical Society, 1996), Vol. 54, pp. 11169.
- [10] John P Perdew, Kieron Burke, and Matthias Ernzerhof, in *Phys. Rev. Lett.* (1996), Vol. 77, pp. 3865.
- [11] G Kresse and D Joubert, in *Phys. Rev. B* (American Physical Society, 1999), Vol. 59, pp. 1758.
- [12] Hendrik J Monkhorst and James D Pack, in *Phys. Rev. B* (American Physical Society, 1976), Vol. 13, pp. 5188.
- [13] C Stephen Hellberg, Kristopher E Andersen, Hao Li, P J Ryan, and J C Woicik, in *Phys. Rev. Lett.* (2012), Vol. 108, p. 166101.
- [14] Q. Qiao, R. F. Klie, S. Ögüt, J. C. Idrobo, *Physical Review B*, 85 (2012) 165406.
- [15] A M Kolpak and S Ismail-Beigi, in *Phys. Rev. B* (2011), Vol. 83, p. 165318.
- [16] PW Peacock and J Robertson, in *Appl Phys Lett* (2003), Vol. 83, pp. 5497.

Heterointegration of III-V on Silicon using a Crystalline Oxide Buffer Layer

ABSTRACT

The integration of III-V compound semiconductors with Si can combine the cost advantage and maturity of Si technology with the superior performance of III-V materials. We have achieved the heteroepitaxial growth of III-V compound semiconductors on a crystalline SrTiO₃ buffer layer grown on Si (001) substrates. A two-step growth process utilizing a high temperature nucleation layer of GaAs, followed by a low-temperature GaAs layer at a higher growth rate was employed to achieve highly crystalline thick GaAs layers on the SrTiO₃/Si substrates with low surface roughness as seen by AFM. The effect of the GaAs nucleation layer on different surface terminations for the SrTiO₃ layer was studied for both on axis and miscut wafers, which led to the conclusion that the Sr terminated surface on miscut substrates provide the best GaAs films. Using GaAs/STO/Si as virtual substrates, we have optimized growth of high quality GaSb using the interfacial misfit (IMF) dislocation array technique. This work can lead to the possibility of realizing infrared detectors and next-generation high mobility III-V CMOS within the existing Si substrate infrastructure.

5.1 INTRODUCTION

The cost effectiveness of silicon combined with the extremely mature processing technology have made silicon one of the most important materials of the 21st century. Even with its cadre of undeniable advantages, the silicon technology still suffers from low optical efficiency and has degraded electrical properties in scaled CMOS devices [1]. On the other hand, III-V semiconductors are ideal candidates for optoelectronic and photonic applications and because of their high carrier mobilities, they are being considered for the channel material in future Si based MOSFETs [2]. However, such implementation would require the monolithic integration of various III-V materials on silicon with low enough defects to fabricate surface channel MOS devices. The integration of III-V compound semiconductors with Si can also combine the cost advantage and maturity of the Si technology with the superior performance of III-V materials resulting in highly integrated semiconductor circuits.

The heterointegration of III-V on Si presents several challenges including the growth of polar on non-polar substrate, high-lattice mismatch and large differences in the coefficients of thermal expansion leading to the formation of anti-phase domain boundaries, dislocations and

surface defects [3]. Various schemes have been used to reduce the density of threading dislocations which include low temperature buffers, superlattice buffers [4] and thermal cycling [5]. Another integration scheme that has been used for GaAs on Si included a crystalline oxide buffer layer, viz. SrTiO₃ that was grown epitaxially on Si [6]. The SrTiO₃ lattice ($a_{STO} = 3.905$ Å) undergoes a 45° rotation to accommodate the high lattice mismatch with the underlying Si (001) ($a_{Si} = 5.431$ Å) leading to a strain of 1.7%. The GaAs lattice ($a_{GaAs} = 5.653$ Å) grown is now strained 2.3% with respect to the 45° rotated SrTiO₃ lattice, thereby enabling the reduction from the original 4% strain for the GaAs/Si system [7]. A two-step growth process utilizing a high temperature nucleation layer of GaAs, followed by a low-temperature GaAs layer at a higher growth rate was employed for this work. The surface termination conditions of the SrTiO₃ crystalline buffer layer have a strong effect on both the crystalline and surface quality of the final GaAs epitaxial growth. Prior work by Largeau *et. al.* has shown the growth of GaAs islands on TiO₂ terminated SrTiO₃ films with the coexistence of wurtzite and cubic phases [8]. This study will investigate the effect of the SrTiO₃ surface terminations on the subsequent GaAs surface and epilayer quality. GaSb is another important III-V material with applications in thermophotovoltaics [9], infrared detectors [10], and low-power high-frequency electronics [11]. The growth of GaSb directly on Si is usually accomplished using an AlSb buffer layer [12]. For this work, the GaAs/STO/Si platform will be used as a virtual substrate for investigating the growth of GaSb layers on Si using the IMF-based growth on GaAs. The IMF array technique relieves the excess strain from the 8% lattice mismatch at the heterointerfaces, leading to the formation of highly crystalline GaSb under the optimized MBE growth conditions. The monolithic integration of GaSb on these Si-based virtual substrates will open up doors for high frequency, low-power tunnel-FETs and Esaki diodes [13]. In this paper we report on the effects of the oxide surface termination on the nucleation and subsequent growth of III-V semiconductors and the use of GaAs/STO/Si as virtual substrates for the growth of GaSb heterostructures.

5.2. EXPERIMENTAL PROCEDURE

The heterointegration approach was developed by growing GaAs films on Si wafers using a crystalline SrTiO₃ buffer layer resulting in templates of GaAs virtual substrates with a potential to grow complex III-V structures on a Si wafer. The concept of this integration was extended by growing GaSb epilayers onto these GaAs templates. Initially, 3" p-Si (001) wafers (on-axis and

4° miscut towards <110>) were treated in a UV-ozone system to aid in the complete removal of carbon contaminants and then loaded into a load-lock section for an initial baking at 150 °C for 30 mins. Then, the wafers were introduced into an oxide MBE chamber equipped with Sr and Ti effusion cells and a molecular oxygen source where 10 nm of SrTiO₃ (STO) with different surface terminations was grown on Si. Prior to the STO buffer layer growth, the Si wafers were cleaned using the de-oxidation procedure as developed by Wei *et al* [14]. The entire growth process was monitored using *in-situ* reflection high electron energy diffraction (RHEED) to determine the growth mode and surface stoichiometry. STO growth was performed in two steps: first a nucleation layer of 2 unit cells was grown on the Si wafer at low temperature (300°C) by co-depositing Sr and Ti under molecular O₂ environment at a partial pressure of 6 x 10⁻⁸ torr followed by a high temperature (550 °C) anneal and subsequent growth of STO using an O₂ partial pressure of 10⁻⁷-10⁻⁶ torr. Typical growth rate used for the oxide film was 1 unit cell/min as determined by RHEED oscillations. Three different surface conditions of the STO film were chosen for this study: stoichiometric, Ti-terminated, and Sr-terminated. By default, the STO growth was performed under a stoichiometric regime (as evidence by a RHEED (1x1) reconstruction) that can be switched to either a Ti-rich or Sr-rich surface by closing the shutter for the respective metal cell and keeping the other one open until specific termination is achieved. The surface termination was monitored by RHEED as detailed in ref. [6]. Following the growth of crystalline STO on Si, all the wafers were unloaded from the MBE cluster tool and stored under ambient conditions. Quarters of STO/Si wafers were then cut and loaded into a III-V MBE chamber for As-based semiconductor growths. Two sets of samples consisting of 0.5 μm and 1.5 μm GaAs were grown on the different STO/Si terminations to show the effect of the STO surface conditions on GaAs epilayer growth. The STO/Si samples were degassed at 580°C for 15 min; then, a GaAs nucleation layer of 25 nm was grown at a temperature of 450 °C using an As₂/Ga ratio of 8 and a growth rate of 0.15 ML/s. Following this, the growth temperature was decreased to 380 °C and 475 nm or 1475 nm of GaAs layer was deposited at an As₂/Ga ratio of 15 and growth rate of 0.5 ML/s. Finally, a post-growth anneal was carried out at 580 °C for 15 minutes with the entire growth process is monitored using *in-situ* RHEED.

The GaAs/SrTiO₃/Si virtual substrates with the best crystalline quality and surface morphologies were then introduced in a different III-V MBE chamber with As and Sb valved

crackers present. Here an additional buffer layer of 0.5 μm GaAs was grown at 580 $^{\circ}\text{C}$ with a growth rate of 0.5 ML/s. Growth rate calibrations were performed previously on a GaAs substrate using RHEED intensity oscillations. Following this, a 0.5 μm layer of GaSb was grown on GaAs at 510 $^{\circ}\text{C}$ using the interfacial misfit (IMF) dislocation array technique as described by Huang *et al* [15]. This technique involves the formation of 90 $^{\circ}$ edge dislocations at the GaAs/GaSb interface, thereby relieving the inbuilt strain mostly at the interface in the form of a 2-D periodic array of misfit dislocations in the [110] and $[\bar{1}10]$ direction. Heteroepitaxial GaSb films of extremely low dislocation density can be achieved using this technique. In this work, The GaSb surface quality was monitored as a function of the V-to-III flux ratios using the IMF array technique. The surface morphology of the grown samples was mapped using atomic force microscopy (AFM) in tapping mode with a Si probe tip and the structural properties of the films were analyzed *ex-situ* using a double crystal X-ray diffractometer.

5.3. RESULTS AND DISCUSSION

The crystallographic orientation of STO with respect Si is such that STO (001)//GaAs(001) and STO[100]//Si[110]. This is made possible as the SrTiO₃ lattice ($a_{\text{STO}} = 3.905 \text{ \AA}$) undergoes a 45 $^{\circ}$ rotation to accommodate the high lattice mismatch with the underlying Si (001) ($a_{\text{Si}} = 5.431 \text{ \AA}$) leading to a mismatch of 1.7%. This results in a critical thickness of approximately 7.6 nm according the Mathews-Blakslee model. Experimentally the critical thickness was found to be around 4nm^{16} , a lower value compared with the model estimation. Fig. 23 displays a typical 10

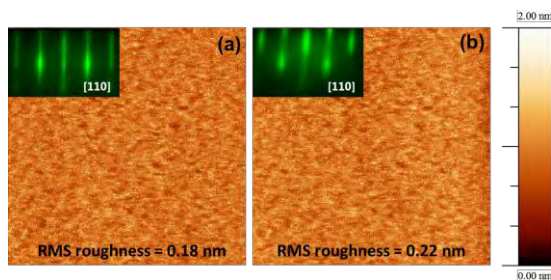


Figure 20: AFM micrographs of 10 nm STO films grown on (a) nominal Si (001) substrate and (b) vicinal 4 $^{\circ}$ miscut Si (001) towards $\langle 110 \rangle$ showing extremely low values of RMS roughness. Inset: RHEED patterns along the [110] direction for each case.

a_{STO} for both wafers. The surface quality is also corroborated *in-situ* by the streaky and sharp

$\mu\text{m} \times 10 \mu\text{m}$ AFM image of 10 nm STO layer grown on both nominal and vicinal 4 $^{\circ}$ miscut Si (001) wafers. The STO undergoes relaxation as it is grown well above the critical thickness on the Si substrate. However, the misfit dislocations accommodate the lattice mismatch between the rotated STO lattice and the underlying Si leading to a surface morphology that exhibits a very flat surface with a root mean square (RMS) roughness of around $\frac{1}{2}$

RHEED patterns displayed in the inset of Fig 23(a) and Fig. 23(b). The different surface terminations of STO exhibit similar features in AFM micrographs and RHEED patterns. These results guarantee that the epitaxy of III-V films on STO/Si template is performed on extremely smooth surfaces.

III-V growth was started with a 25 nm of GaAs nucleation layer. Diffraction patterns at the end of the nucleation layer along $[\bar{1}10]$ azimuth are shown for the Ti- and Sr-terminated STO films in Fig. 24.

Both RHEED patterns are spotty indicating 3 dimensional growth of the nucleation layer with the formation of islands. The RHEED pattern of the GaAs nucleation layer grown on

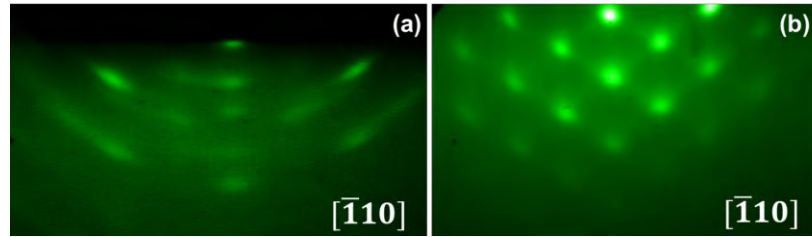


Figure 22: RHEED patterns observed along the $[\bar{1}10]$ direction during the GaAs nucleation layer growth on (a) Ti-terminated STO and (b) Sr-terminated STO.

the Ti-terminated STO surface is spotty with ring-like features suggesting a polycrystalline nature of this layer, i.e. crystal grains with several orientations where, possibly, cubic and

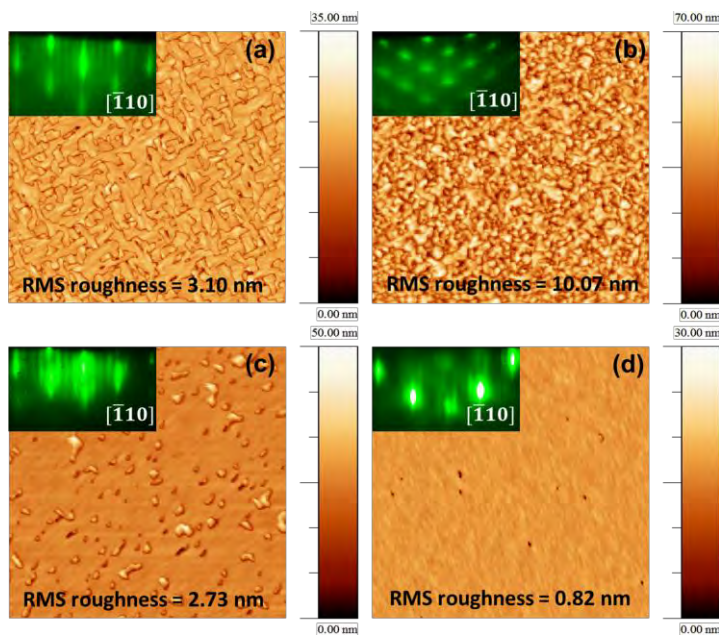


Figure 21: AFM scans of $10 \mu\text{m} \times 10 \mu\text{m}$ areas of the GaAs film surface on (a) nominal STO/Si(001) (b) Ti-terminated STO/miscut Si(001) (c) stoichiometric STO/miscut Si(001) (d) Sr-terminated STO/miscut Si(001). Inset: RHEED patterns along the $[\bar{1}10]$ direction for each case.

hexagonal phases could coexist (Fig. 24(a)). On the other hand, the nucleation on the Sr-terminated surface shows a well-ordered spotty RHEED pattern where the diffraction spots arrangement and interconnection is indicative of cubic monocrystalline faceted islands (Fig. 24(b)). Similar to this, the nucleation on stoichiometric STO exhibits the same behavior. From RHEED patterns, it is evident that the crystallographic relationship STO (001)//GaAs(001) and STO[100]//Si[110] exists

confirming the 45° rotation of STO w.r.t to both the underlying Si and overlying GaAs epilayer.

GaAs films grown on STO show a strong dependency on the miscut of the Si substrate (on axis and offcut), the thickness of GaAs and the underlying termination of the STO as can be observed in AFM images of Fig. 25. In this figure, the topography of 1.5 μm thick GaAs film in a 10 μm x 10 μm AFM scan is shown as a function of these parameters. GaAs grown on on-axis STO/Si(001) presents a surface morphology consisting of clear antiphase domains that are isolated by well-defined boundaries (Fig. 25(a)) resulting, in general, from the heteroepitaxy of polar semiconductors grown on a nonpolar surfaces as in this case where the GaAs is grown on STO(001)/Si surface with no miscut on the starting Si substrate. Although the RMS roughness is high in this sample (~ 3.1 nm), the individual domains exhibit very flat surfaces as is corroborated by the 4x streaky and slightly spotty RHEED pattern (inset of Fig. 25(a)). RHEED also confirms, in this sample, the 2-domain nature as seen in the AFM micrograph in which the 4x reconstruction from the (2x4) surface is present in the orthogonal [110] azimuths. The growth on miscut STO/Si templates promotes the growth of single domain GaAs as evidenced in AFM images (Figs. 25(c) and 25(d)), however, the growth is strongly dependent on the STO surface termination. GaAs grown on Ti-terminated STO surface depicts a grainy topography with a high RMS roughness of ~ 10 nm (Fig 25(b)), this texture is in agreement with the spotty RHEED obtained at the end of the growth in inset of Fig. 25(b). On the other hand, GaAs layer grown on stoichiometric and Sr-terminated display flatter surfaces where antiphase domains are absent (Fig. 25(c) and 25(d)). Also, the RMS roughness has improved from 10 nm to as low as 2.7 nm and 0.8 nm for stoichiometric and Sr-rich surfaces, respectively. The stoichiometric termination shows a GaAs film mainly being flat but with small mound grains and holes that contributes to the roughness while GaAs on Sr-terminated STO surface is characterized by a very flat topography with just a few small holes and the lowest roughness a necessary requirement for device fabrication. The streaky RHEED patterns (insets Fig 25(c) and 25(d)) are in correspondence with the observed surface features in both samples; (2x4) surface reconstruction is clearly seen at the growth temperature. In particular, the sample with the lowest roughness displays a RHEED pattern whose diffraction features are along a semicircle indicative of a very smooth surface. XRD analysis was performed for the sample with the optimum surface quality according to AFM. Diffraction peaks are clearly observed from relaxed (200) STO planes and relaxed (200) and (400) GaAs lattice planes (Fig. 26). The wafer miscut inhibits the detection of

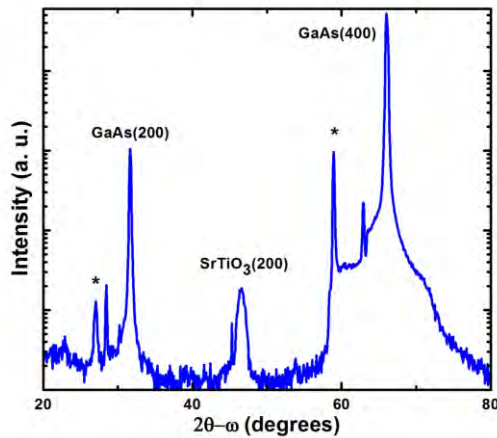


Figure 23: Coupled 2Theta-omega XRD scan for GaAs grown on Sr-terminated STO/miscut Si (001) substrate. The symbol “*” represents the peaks arising from the $Cu-k_{\beta}$ x-ray emission. The extra sharp peaks are related to instrument noise.

order for GaAs to wet the STO surface properly leading eventually to a 2D growth mode, the surface energy of the STO surface should be greater than the sum of the GaAs surface energy and the interface energy. The surface energy of a Sr-terminated STO surface has been calculated to be 1433 erg/cm^2 according to Zhang *et al* [17]. The surface energy of different GaAs (100) reconstructions have also been calculated using *ab initio* density functional methods, and for $\beta 2(2 \times 4)$ reconstruction, this value is around 1000 erg/cm^2 according to Haugk *et al* [18]. Recent calculations by Demkov *et al* have shown that the interface energy for this system can be as low as 300 erg/cm^2 , which implies that, in theory, the Sr-terminated STO provides enough energy to the surface to exceed the sum of the GaAs surface energy and the interface energy [19]. This

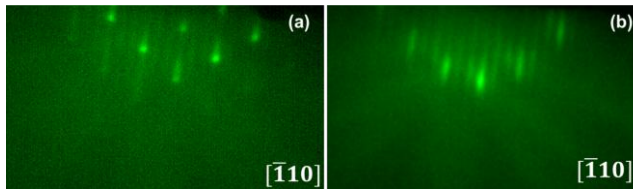


Figure 24: RHEED patterns observed along the $[\bar{1}10]$ direction during the GaSb growth on Ga-rich GaAs surface (a) initial stages showing GaSb islands and 2D growth and (b) (1×3) reconstruction after 50 nm GaSb showing two-dimensional growth.

the Si (400) planes since the Bragg condition is no longer satisfied in this orientation of the substrate.

We observe, that the best results for surface roughness (0.8 nm) are obtained for GaAs films grown on a Sr-terminated STO buffer layer for a $1.5 \mu\text{m}$ thick layer on Si (001) with a 4° miscut in the $\langle 110 \rangle$ direction. As mentioned before, the crystalline quality and surface morphology of the GaAs epilayer depends strongly on the surface energy of the STO film which is governed by the surface termination. In

leads to complete wetting of the GaAs layer and subsequent layer-by-layer growth responsible for high crystalline quality and optimum surface quality. As compared to the Ti-terminated STO, the surface energy is not enough to overcome this sum and leads to the formation of polycrystalline films which do not exhibit

the 2D growth mode and are much rougher than the Sr-terminated case.

For the integration of GaSb onto silicon needed for the development of high mobility transistors in the next generation CMOS applications, the GaAs/STO/Si virtual substrate platform was used. Here a buffer layer of GaAs was first grown onto the GaAs/SrTiO₃/Si(001) virtual substrate with a 4° miscut in the <110> direction leading to a clear (2 x 4) reconstruction at a substrate temperature of 580 °C. The surface was then Ga-stabilized leading to a (4 x 2) reconstruction by closing the As shutter. At this point, the introduction of Sb flux leads to a (2 x 8) reconstruction

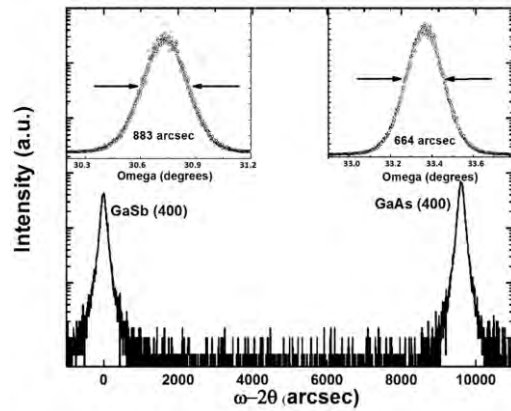


Figure 26: Triple-axis omega-2theta scan for GaAs (400) and GaSb (400) showing complete relaxation of the GaSb epilayer and narrow FWHM for both peaks indicating high crystalline quality layers. Inset: Rocking curves for GaSb and GaAs (400) peaks.

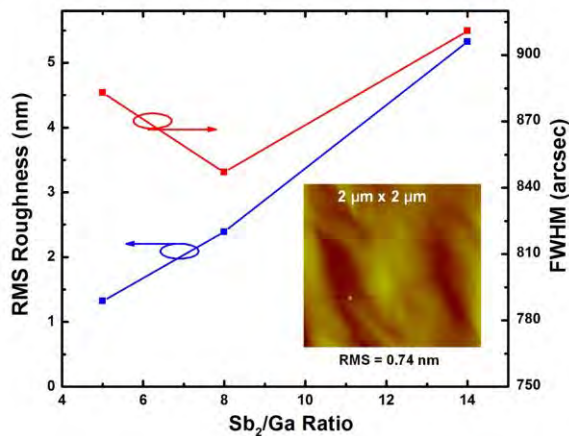


Figure 25: RMS surface roughness of 10 μm x 10 μm areas and GaSb (400) rocking curve FWHM mapped as a function of Sb₂/Ga flux ratio. Inset: AFM micrograph of a 2 μm x 2 μm area showing extremely smooth surface quality for a flux ratio of 5

layer by layer growth as in Fig. 27(b).

Fig. 28 shows the triple-axis omega-2theta scan for the GaAs (400) and GaSb (400) peaks which reveal a completely relaxed GaSb layer with respect to the underlying GaAs. The inset for this figure shows the respective omega rocking curves for GaSb and GaAs with FWHM values of

indicating atomic packing instead of tetragonal distortion, resulting in 90° pure edge dislocations for the formation of the IMF dislocation array. The substrate was then cooled down to 510 °C while maintaining the (2 x 8), and the GaSb deposition was then resumed with the growth showing Stranski-Krastanov (SK) mode as observed in the RHEED patterns for figure 27. Fig. 27(a) shows island growth after an initial thin layer of GaSb and as growth commences, the islands coalesce and the RHEED transforms into a clear (1 x 3) surface reconstruction depicting

883 arcsec and 664 arcsec respectively indicating high crystalline quality with low density of dislocations in these films. To optimize the parameters for high quality growth of GaSb on the silicon-based virtual substrates, different V-III flux ratios were used; this was determined by measuring the beam equivalent pressures (BEP) using an ion gauge. Fig. 29 summarizes the rocking curve FWHM of the GaSb (400) peaks as a function of Sb/Ga flux ratio. AFM scans of $10\ \mu\text{m} \times 10\ \mu\text{m}$ areas were also performed for all the samples to determine the growth parameters needed to produce the lowest RMS roughness, also shown in Fig. 29. The data shows that the minimum surface roughness was obtained for a V-III flux ratio of 5 and the optimum FWHM was obtained for a ratio 8 suggesting there is a growth window present for high surface and epilayer quality between the Sb_2/Ga flux ratios of 5 and 8.

5.4. CONCLUSION

We have successfully demonstrated high quality growth of GaAs on SrTiO_3/Si substrates using solid-source MBE. The crystalline and surface quality of the GaAs films were monitored as a function of the surface termination of the STO layer. The Sr-terminated STO surface has sufficient surface energy to allow for wetting and 2D growth of the GaAs film and produces the best surface morphologies. Using the GaAs/STO/Si wafers as virtual substrates, GaSb films were grown on the Ga-rich GaAs surface via the IMF array technique. The growth of GaSb was optimized to achieve films with high crystalline quality and extremely low RMS surface roughness values using AFM. Successful monolithic integration of GaAs and GaSb on Si can lead to future III-V low cost CMOS devices as well as multifunctional devices on a single Si chip.

References

- [1] Taur Yuan, D. A. Buchanan, Chen Wei, D. J. Frank, K. E. Ismail, Lo Shih-Hsien, G. A. Sai-Halasz, R. G. Viswanathan, H. J. C. Wann, S. J. Wind, and Wong Hon-Sum, *Proc. IEEE* **85** (4), 486 (1997).
- [2] Jesus A. del Alamo, *Nature* **479** (7373), 317 (2011).
- [3] S. H. Huang, G. Balakrishnan, A. Khoshakhlagh, L. R. Dawson, and D. L. Huffaker, *Appl. Phys. Lett.* **93** (7), 3 (2008).
- [4] T. Soga, S. Hattori, S. Sakai, M. Takeyasu, and M. Umeno, *J. Appl. Phys.* **57** (10), 4578 (1985).

- [5] Y. Itoh, T. Nishioka, A. Yamamoto, and M. Yamaguchi, *Appl. Phys. Lett.* **52** (19), 1617 (1988).
- [6] R. Droopad, Z. Y. Yu, H. Li, Y. Liang, C. Overgaard, A. Demkov, X. D. Zhang, K. Moore, K. Eisenbeiser, M. Hu, J. Curless, and J. Finder, *Journal of Crystal Growth* **251** (1-4), 638 (2003).
- [7] K. Eisenbeiser, R. Emrick, R. Droopad, Z. Yu, J. Finder, S. Rockwell, J. Holmes, C. Overgaard, and W. Ooms, *Ieee Electron Device Letters* **23** (6), 300 (2002).
- [8] L. Largeau, J. Cheng, P. Regreny, G. Patriarche, A. Benamrouche, Y. Robach, M. Gendry, G. Hollinger, and G. Saint-Girons, *Appl. Phys. Lett.* **95** (1), 011907 (2009).
- [9] A. S. Licht, D. F. Demeo, J. B. Rodriguez, and T. E. Vandervelde, in *Physics, Simulation, and Photonic Engineering of Photovoltaic Devices Iii*, edited by A. Freundlich and J. F. Guillemoles (Spie-Int Soc Optical Engineering, Bellingham, 2014), Vol. 8981.
- [10] E. H. Aifer, E. M. Jackson, G. Boishin, L. J. Whitman, I. Vurgaftman, J. R. Meyer, J. C. Culbertson, and B. R. Bennett, *Appl. Phys. Lett.* **82** (25), 4411 (2003).
- [11] B. R. Bennett, R. Magno, J. B. Boos, W. Kruppa, and M. G. Ancona, *Solid-State Electron.* **49** (12), 1875 (2005).
- [12] G. Balakrishnan, S. Huang, L. R. Dawson, Y. C. Xin, P. Conlin, and D. L. Huffaker, *Appl. Phys. Lett.* **86** (3), 3 (2005).
- [13] D. Pawlik, B. Romanczyk, P. Thomas, S. Rommel, M. Edirisooriya, R. Contreras-Guerrero, R. Droopad, W. Y. Loh, M. H. Wong, K. Majumdar, W. E. Wang, P. D. Kirsch, and R. Jammy, presented at the Electron Devices Meeting (IEDM), 2012 IEEE International, 2012 (unpublished).
- [14] Wei Yi, Xiaoming Hu, Yong Liang, D. C. Jordan, Brad Craigo, Ravi Droopad, Z. Yu, Alex Demkov, John L. Edwards, and William J. Ooms, *Journal of Vacuum Science & Technology B: Microelectronics and Nanometer Structures* **20** (4), 1402 (2002).
- [15] S. H. Huang, G. Balakrishnan, and D. L. Huffaker, *J. Nanosci. Nanotechnol.* **11** (6), 5108 (2011).
- [16] J. C. Woicik, H. Li, P. Zschack, E. Karapetrova, P. Ryan, C. R. Ashman, and C. S. Hellberg, *Physical Review B* **73** (2), 024112 (2006).
- [17] X. Zhang, A. A. Demkov, Hao Li, X. Hu, Yi Wei, and J. Kulik, *Physical Review B* **68** (12), 125323 (2003).
- [18] M. Haugk, J. Elsner, and Frauenheim Th, *Journal of Physics: Condensed Matter* **9** (35), 7305 (1997).
- [19] A. A. Demkov, H. Seo, X. Zhang, and J. Ramdani, *Applied Physics Letters* **100** (7), 071602 (2012).

AFOSR Deliverables Submission Survey

Response ID:4787 Data

1.

1. Report Type

Final Report

Primary Contact E-mail

Contact email if there is a problem with the report.

rdroopad@txstate.edu

Primary Contact Phone Number

Contact phone number if there is a problem with the report

5122456165

Organization / Institution name

Texas State University

Grant/Contract Title

The full title of the funded effort.

Heterointegration of Dissimilar Materials

Grant/Contract Number

AFOSR assigned control number. It must begin with "FA9550" or "F49620" or "FA2386".

FA9550-10-1-0133

Principal Investigator Name

The full name of the principal investigator on the grant or contract.

Ravi Droopad

Program Manager

The AFOSR Program Manager currently assigned to the award

Kenneth Goretta

Reporting Period Start Date

05/01/2010

Reporting Period End Date

04/30/2015

Abstract

The integration scheme for compound semiconductors, functional oxides and silicon has been developed using molecular beam epitaxy with the oxide as a buffer layer on silicon substrates. This scheme will enable multifunctional oxides to be integrated with Si based logic and high speed optoelectronics afforded by III-V compound semiconductors. Various processes were developed whereby functional oxides were epitaxially deposited onto both silicon and compound semiconductor substrates. The oxide/semiconductor interface was studied in an effort to understand the bonding chemistry and the energetics to develop growth processes for 2-dimensional growth of compound semiconductors. Using a combination of high resolution transmission electron microscopy, in-situ XPS and density functional calculation a model of the bonding between the atoms at the SrTiO₃/GaAs interface emerge. The relative stability of a number of interfacial structures was compared using the Gibbs free energy and for thin oxide layers, the most energetically stable structure was determined to be As-Sr interface

DISTRIBUTION A: Distribution approved for public release

with Sr atoms coming from an oxygen-depleted SrO layer. Using 3 terminations of the oxide surface, compound semiconductor layers were deposited by MBE.

Distribution Statement

This is block 12 on the SF298 form.

Distribution A - Approved for Public Release

Explanation for Distribution Statement

If this is not approved for public release, please provide a short explanation. E.g., contains proprietary information.

SF298 Form

Please attach your SF298 form. A blank SF298 can be found [here](#). Please do not password protect or secure the PDF. The maximum file size for an SF298 is 50MB.

[SF298.pdf](#)

Upload the Report Document. File must be a PDF. Please do not password protect or secure the PDF. The maximum file size for the Report Document is 50MB.

[AFOSR Final report.pdf](#)

Upload a Report Document, if any. The maximum file size for the Report Document is 50MB.

Archival Publications (published) during reporting period:

Carrier-mediated ferromagnetism in SrTi_{1-x}Fe_xO₃, Chun-Lan Ma, Byounghak Lee, Rocio Contreras-Guerrero, Ravi Droopad, and Allan H. MacDonald, in preparation

Structural Properties of SrTiO₃ on GaAs(001) Interface, Joelson Cott-Garcia, Rocio Contreras-Guerrero, Qiao Qiao, Liang Hong, Serdar Ogut, Ravi Droopad, Robert F. Klie, and Byounghak Lee, in preparation

Direct Observation of oxygen-vacancy-enhanced polarization in SiTiO₃-buffered ferroelectric BaTiO₃ film on GaAs, Qiao Qiao, Yuyang Zhang, Rocio Contreras-Guerrero, Ravi Droopad, Sokrates T. Pantelides, Stephen J. Pennycook, Serdar Ogut, Robert F. Klie, submitted to Advanced Electronic Materials

Functional materials integrated on III–V semiconductors, Javad Gatabi, Kevin Lyon, Shafiqur Rahman, Manuel Caro, Juan Rojas-Ramirez, Joelson Cott-Garcia, Ravi Droopad, Byounghak Lee, Microelectronic Engineering 147 (2015) 117–121

Electrical and Optical Properties of LiNbO₃/CaCu₃Ti₄O₁₂ heterostructures on Si, Javad R. Gatabi, Kevin A. Lyon, Shafiqur Rahman, Hanu Arava, Juan S Rojas-Ramirez, R. K. Pandey, Ravi Droopad, to be published in MRS proceedings, 2015

Heterointegration of III–V on silicon using a crystalline oxide buffer layer, K. Bhatnagar, J.S. Rojas-Ramirez, R. Contreras-Guerrero, M. Caro, R. Droopad, Journal of Crystal Growth, 425, (2015), 262–267

Properties of epitaxial BaTiO₃ deposited on GaAs, R. Contreras-Guerrero, J. P. Veazey, J. Levy, and R. Droopad, Appl Phys Letts. 102 (2013) 012907

Interface properties of MBE grown epitaxial oxides on GaAs, R. Contreras-Guerrero, M. Edirisooriya, O.C. Noriega, R. Droopad, Journal of Crystal Growth 378 (2013) 238–242

Magnetic and Structural Properties for epitaxial growth of BiFeO₃ thin films on SrTiO₃/Si(100) substrates, R. Laughlin, D. Currie, R. Contreras-Guerrero, A. Dedigama, W. Priyantha, R. Droopad, N. Theodoropoulou, P. Gao, X. Pan, J. Appl. Phys. 113, 17D919 (2013)

Epitaxial ferroelectric oxides on semiconductors- A route towards negative capacitance devices, R. Droopad, R. Contreras-Guerrero, J.P. Veazey, Q. Qiao, R.F. Klie, J. Levy, Microelectronic Engineering, 109, (2013) 290-293.

Theory of t_{2g} electron-gas Rashba interactions, G. Khalsa, B. Lee, A.H. MacDonald, Phys. Rev. Letts. 88 (2013) 41302.

Atomic-layer-deposited LaAlO₃/SrTiO₃ all oxide field-effect transistors, Dong, L.; Liu, Y. Q., Xu, M., Wu, Y. Q., Colby, R., Stach, E. A., Droopad, R., Gordon, R. G., Ye, P. D., International Electron Device Meeting- Technical Digest, 2010

Changes in research objectives (if any):

None

Change in AFOSR Program Manager, if any:

DISTRIBUTION A: Distribution approved for public release

Program Manager changed from Dr. Kitt Reinhardt, to Dr. James Hwang and finally to Dr. Kenneth Goretta

Extensions granted or milestones slipped, if any:

none

AFOSR LRIR Number

LRIR Title

Reporting Period

Laboratory Task Manager

Program Officer

Research Objectives

Technical Summary

Funding Summary by Cost Category (by FY, \$K)

	Starting FY	FY+1	FY+2
Salary			
Equipment/Facilities			
Supplies			
Total			

Report Document

Report Document - Text Analysis

Report Document - Text Analysis

Appendix Documents

2. Thank You

E-mail user

Jul 22, 2015 14:18:55 Success: Email Sent to: rdroopad@txstate.edu

Response ID: 4787

Survey Submitted:	Jul 22, 2015 2:18 PM
IP Address:	147.26.174.105
Language:	English (en-US,en;q=0.5)
User Agent:	Mozilla/5.0 (Windows NT 6.1; WOW64; rv:39.0) Gecko/20100101 Firefox/39.0

Http Referrer:	http://afosr.reports.sgizmo.com/s3/
Page Path:	1 : (SKU: 1) 2 : Thank You (SKU: 2)
SessionID:	1437588497_55afdc11af3826.45358610

Response Location

Country:	United States
Region:	TX
City:	San Marcos
Postal Code:	78666
Long & Lat:	Lat: 29.872900009155, Long:-98.013999938965